RSC Applied Polymers

Accepted Manuscript

This article can be cited before page numbers have been issued, to do this please use: P. Rajaee, I. Wijesinghe, Z. Li and C. Yan, *RSC Appl. Polym.*, 2025, DOI: 10.1039/D5LP00189G.

ROYAL SOCIETY OF CHEMISTRY

rsc.li/RSCApplPolym

View Article Online
DOI: 10.1039/D5LP00189G

Recent advances in polymeric materials with exceptional mechanical performance via multiple hydrogen-bonded networks

Pouya Rajaee[1,2], Ishara Wijesinghe[1,2], Zhiyong Li[1,2], Cheng Yan[1,4*]

[1]School of Mechanical, Medical, and Process Engineering, Faculty of Engineering, Queensland University of Technology, 2 George Street, Brisbane, QLD 4000, Australia.
[2]Centre for Biomedical Technologies, Queensland University of Technology, 2 George Street, Brisbane, QLD 4000, Australia.
[3]Faculty of Animal Science and Export Agriculture, Uva Wellassa University of Sri Lanka, Passara Road, Badulla, 90000, Sri Lanka.
[4]Centre for Materials Science, Queensland University of Technology, 2 George Street, Brisbane, QLD 4000, Australia.

*Corresponding Author: Cheng Yan (c2.yan@qut.edu.au)

Contact details of authors:

- Pouya Rajaee: pouya.rajaee@hdr.qut.edu.au
- Ishara Wijesinghe: ishara.gedara@hdr.qut.edu.au
- Zhiyong Li: zhiyong.li@qut.edu.au
- Cheng Yan: c2.yan@qut.edu.au

Abstract

The development of lightweight polymeric materials with high strength and toughness is a growing research focus. Traditional chemical cross-linking techniques, while improving

strength, generally compromise toughness. Particle-based cross-linkers, including small molecules, nanoparticles, or polymer aggregates, on the other hand, can form multiple hydrogen-bonded networks with polymer chains, thereby simultaneously enhancing strength and toughness. In addition to highlighting recent advancements in engineering such networks, this short review addresses the effects of different particle types on the mechanical properties of polymers and highlights key design strategies, performance improvements, and industrial opportunities.

Keywords

Polymeric materials; Particle-based cross-linkers; Multiple hydrogen-bonded networks; Mechanical properties.

1. Introduction

The development of lightweight, strong, tough, and self-healing polymeric materials has drawn increased attention from researchers recently due to their wide applications in manufacture, flexible electronics, transportation, packaging, energy storage and conversion, and biomedical engineering [1–9]. However, achieving a balance between strength and toughness is typically a challenge in polymeric materials, as compared to metallic and ceramic materials [10,11]. This difficulty arises from the classic dilemma of mutually exclusive strength and toughness in most materials.

Introducing dynamic covalent bonds, such as disulphide, oxime ester, imine, borate ester, and others, is an effective way to enable self-healing in molecular structures. Dynamic covalent bonding has been found to significantly speed up healing and increase healing efficiency [12–15]. However, due to the distinct molecular interactions, this process often results in reduced extensibility [16–19]. In contrast, dynamic non-covalent cross-linking, including hydrogen bonds (H-bonds), in polymeric materials can increase strength without compromising toughness and ductility [20–29]. Despite having a lower bond energy than covalent bonds, multiple non-covalent bonds can dramatically alter the structures and properties of polymeric materials [30]. It is primarily through nanoconfinement, a process enabled by multiple non-covalent bonds, that the overall properties of polymeric materials are enhanced [31].

The dissociation and restoration of H-bonds under mechanical strain distribute the energy of fractures across molecules, leading to self-deformation and exceptional toughness. This finding provides a fundamental design strategy for effectively manufacturing materials with super high performance using multiple hydrogen bonds [32,33].

View Article Online
DOI: 10.1039/D5LP00189G

Recent advancements in multiple H-bonds have demonstrated promising ways to enhance mechanical strength, toughness, and healing capabilities without sacrificing material flexibility. In this review, the term "multiple hydrogen-bonded networks" refers to cross-linked polymer systems in which multiple H-bonds are formed with polymer chains by additional particles, such as small molecules, nanoparticles, or polymer aggregates. Such particles act as cross-linkers, providing self-healing, structural stability, and energy dissipation by forming reversible non-covalent bonds between polymer chains. Looking ahead to the future of polymeric materials, this short review explores the most recent advancements in high-performance polymeric materials via such networks. Finally, we draw conclusions and present a detailed analysis of the challenges and prospects in the development of hydrogen bond cross-linked polymeric materials.

2. Hydrogen bond and its effect on mechanical behaviour

H-bonds are a common type of intermolecular force in nature and are important to many biological processes, such as protein folding and DNA replication [34,35]. The basic structure of a hydrogen bond, X−H···Y, comprises a proton donor (X−H, abbreviated as D) and a proton acceptor (Y atom having lone pair electrons, abbreviated as A). Hydrogen bonds form when two electronegative atoms are attracted to each other. This bonding interaction occurs because of the electrostatic attraction among the negatively charged Y atom (δ^-) and the positively charged hydrogen (δ^+ X−H), and the interaction of a lone pair of electrons from the electron-rich Y atom with the σ-antibonding orbital of the X−H bond [36].

A single hydrogen bond is more powerful than van der Waals forces but not as strong as covalent bonds. The strength of hydrogen bonds can vary significantly depending on factors such as bond angle, distance between atoms, and the electronegativity of the involved atoms, ranging from near-covalent bonds to extremely dynamic interactions [37–45]. In supramolecular bonds, hydrogen bonds have comparatively weak and erratic individual strengths. Consequently, highly dynamic hydrogen bonds are often used to create polymeric materials with good self-healing characteristics but lower strength and stiffness. While H-bonds can produce polymeric materials with performance comparable to covalent polymers, the stability of these bonds requires additional energy to break and reform new hydrogen bonding networks. Thus, while strong hydrogen bonds can produce robust polymeric materials, they may compromise self-healing abilities. To achieve a balance between strength and self-healing capability, multiple hydrogen bonds are of significant interest [46–48].

View Article Online
DOI: 10.1039/D5LP00189G

3. Polymeric materials with multiple hydrogen-bonded networks

Adding particle-based cross-linkers is a crucial method for producing polymeric materials with hydrogen-bonded networks. Kawakami et al. [49] utilized small bispyridine molecules for liquid-crystalline, increasing mesophase stability. Cross-linkers have since been developed (see Figure 1). These cross-linkers can improve the properties of polymers through multiple H-bonding.

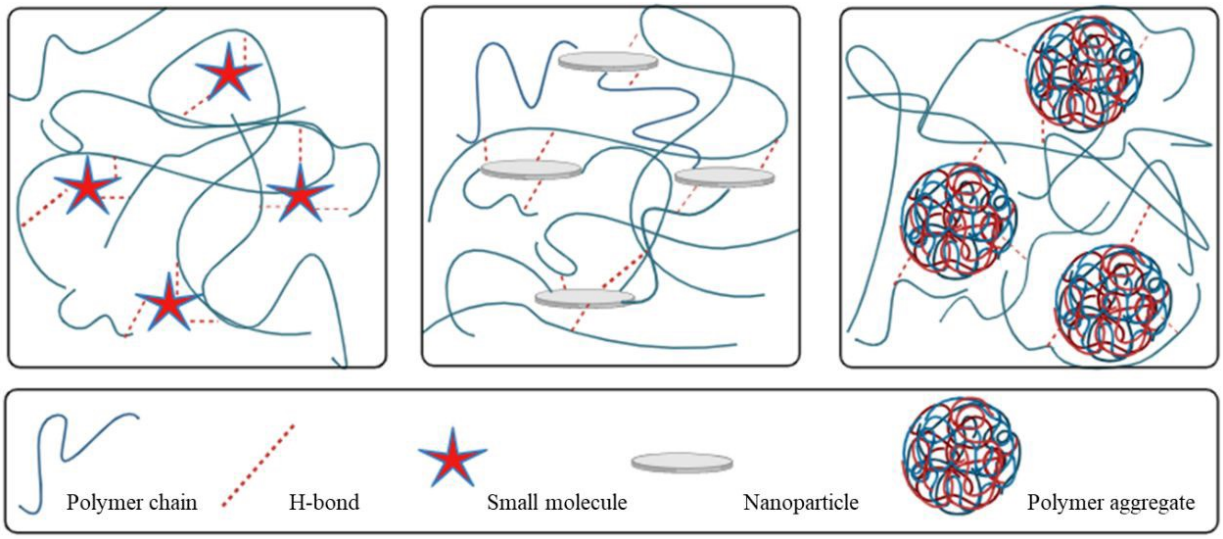

Figure 1. The H-bond cross-linking of polymeric materials by small molecules, nanoparticles, or polymer aggregates.

3.1.The role of small molecules

Small molecules rich in groups containing oxygen, nitrogen or fluorine can be effective cross-linkers in polymers. For example, Liu et al. [50] prepared HCPA as a hydrogen-bonded cross-linker for polyvinyl alcohol (PVA), resulting in strong, tough, and self-healable polymeric materials. HCPA, consisting of six amino molecules, formed a strong supramolecular structure within PVA by physically cross-linking PVA chains through multiple hydrogen bonds (Figure 2a). Increase of HCPA greatly improved the tensile characteristics of PVA: strain at break increased by 173%, toughness by 370%, and tensile strength by 48% at 5 wt.% HCPA (Figure 2b). These findings clearly show that HCPA could simultaneously toughen and strengthen PVA, proven to be extremely challenging because of the mutually exclusive mechanisms governing toughness and strength.

The toughening and reinforcing mechanisms of HCPA in PVA were investigated using small-angle X-ray scattering (SAXS) measurements and inspection of the fracture morphologies (Figures 2c-e). When PVA/HCPA was stretched to 100%, the 2D scattering pattern displayed

View Article Online
DOI: 10.1039/D5LP00189G

a size increase and the formation of a wide, loose scattering ring, showing the deformation of HCPA-cross-linked nanodomains. When tensile strain increases, the scattering peak in PVA/HCPA shifted to smaller scatter vectors (q), while PVA showed no significant change. The Guinier radius (R_g) of the H-bonded nanodomains rose steadily, from nearly 22 nm at 0% strain to nearly 30 nm at 100% strain. This characteristic, which efficiently dissipates energy and inhibits the formation and propagation of microcracks, allowing the nanodomains to grow when stretched by breaking and rapidly reconstructing H-bonds between HCPA and PVA [51]. In addition, in contrast to the smooth surface of PVA, the PVA/HCPA fracture morphologies following tensile testing exhibited large-crinkled, network-like structures. This indicates that HCPA-crosslinked nanodomains cause matrix deformation, aiding in the absorption and dissipation of stress energy.

Experimental validation through infrared (IR) spectroscopy, rheological studies, creep and recovery tests, and differential scanning calorimetry (DSC) confirmed the formation of robust hydrogen bonds between HCPA and PVA, evident from IR spectroscopy where noticeable blue shifts were observed in hydroxyl group upon the addition of HCPA [51–55] (Figure 2f). Rheological investigations revealed a unique 'second plateau' feature of a hydrogen bond-formed cross-linked network [56–59] (Figure 2g). Lower creep rates were observed in PVA/HCPA during creep and recovery testing, indicating a robust H-bond crosslink network that reduces deformation over time [60] (Figure 2h). Thermal analysis showed that the movement of PVA chains was significantly limited by strong H-bonds with HCPA, as indicated by the initial increase in the glass transition temperature (T_g) of PVA with HCPA [61–63] (Figure 2i). At higher concentrations, there were also slight depressions in T_g, which could isolate PVA chains and weaken interchain interactions, thereby promoting segmental mobility [56].

Excellent self-healing properties were also observed by PVA/HCPA (Figure 2j-n). The initial mechanical strength of these films was significantly reduced upon puncture. However, nearly complete recovery occurred when a small amount of H_2O was applied to the damaged region, and the film was left to heal at ambient temperature for 24 h. The healed films greatly outperformed PVA without HCPA, regaining almost 99% of their strength and over 91% of their break strain. Comparable results were also observed with cut damage; after the application of water and subsequent healing, break strain and tensile strength returned by more than 69% and over 93%, respectively, surpassing the recovery rates of PVA.

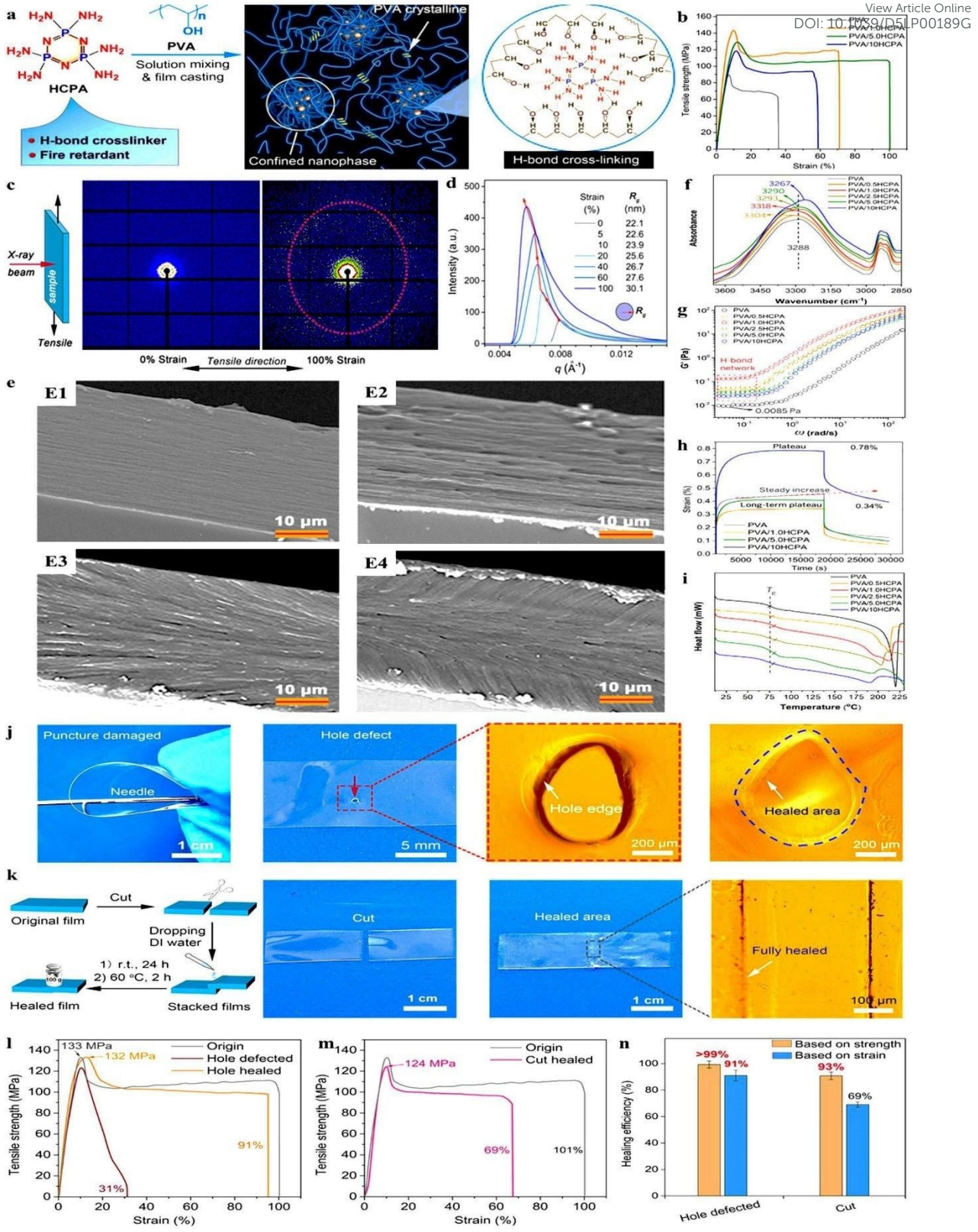

Figure 2. (a) Diagram showing the synthesis of HCPA as a hydrogen-bonded cross-linker and the process for creating supramolecular PVA/HCPA. (b) Stress-strain curves for PVA/HCPA films. (c) 2D SAXS patterns of PVA with 5 wt.% HCPA at 0% and 100% strain. (d) SAXS data illustrating the R_g of nanodomains as a function of tensile strain. (e) Scanning

View Article Online
DOI: 10.1039/D5LP00189G

electron microscope (SEM) images of fracture cross-sections of (E1) PVA, (E2) PVA with 1 wt.% HCPA, (E3) PVA with 5 wt.% HCPA, and (E4) PVA with 10 wt.% HCPA after tensile testing. (f) IR spectra for PVA and PVA/HCPA, (g) frequency dependence of G′ for 5 wt.% aqueous solutions, (h) creep and recovery curves for PVA and PVA/HCPA, (i) DSC curves for PVA and PVA/HCPA. (j) Digital and optical photos of films with puncture damage before and after 24-hour healing at room temperature. (k) Diagram showing cut damage and healing processes, with digital and optical photos of films before and after 24-hour healing at room temperature and 2 hours at 60°C. (l, m) Stress-strain curves before and after healing, and (n) healing efficiency. (a-n) Reproduced with permission [50].

Liu et al. [64], in another study, developed PVA that combines great toughness, high ductility, and substantial strength using β-cyclodextrin (β-CD) as a hydrogen-bonded cross-linker (Figure 3a). They investigated how this cross-linker affected the mechanical properties of PVA (Figure 3b). Initially, PVA exhibited a modulus of about 2 GPa and a strength of 113 MPa. With an increase in β-CD to 1 wt.%, tensile strength and elastic modulus increase to 136.5 MPa and 3 GPa, respectively. The breaking strain and toughness reached their maximum at 2 wt.% β-CD, increased by 397% and 481% over PVA, respectively. However, higher β-CD levels led to reduced mechanical performance due to β-CD cluster formation decreasing effective hydrogen bonding with PVA. The robust hydrogen bond interactions between β-CD and PVA chains were confirmed by IR spectroscopy, X-ray photoelectron spectroscopy (XPS), DSC, rheological tests, and X-ray diffraction (XRD). For instance, XPS spectra showed that adding β-CD caused the PVA C1s peak to shift to higher binding energy, indicating hydrogen bond interactions between PVA and β-CD [65,66] (Figure 3c). The higher C−O content in β-CD resulted in an enhanced ratio of C−C to C−O in PVA with 5 wt.% β-CD compared to PVA. XRD analysis using 2 wt.% β-CD revealed a decrease in the crystalline size of PVA compounds from 5.33 to 4.25 nm, as hydrogen bond interactions prevented PVA chain rearrangement during crystallization [67] (Figure 3d). A higher β-CD content marginally increased crystalline size, likely due to PVA bonds being weakened by β-CD aggregation [68].

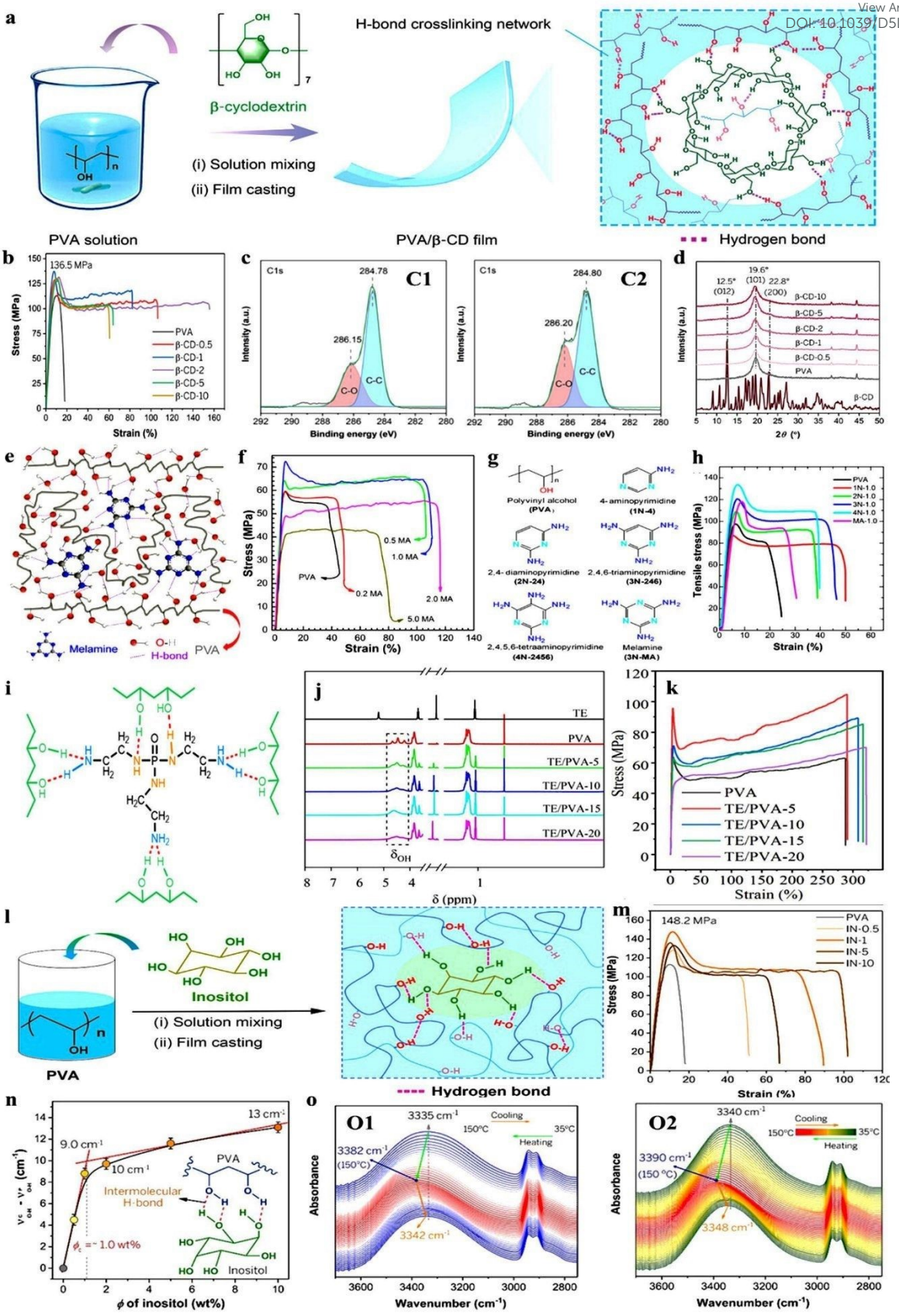

Figure 3. (a) Diagram illustrating the preparation method for PVA/β-CD films. (b) Stress-strain curves for PVA/β-CD films. (c) High-resolution C1s elemental scans for (C1) PVA and

View Article Online
DOI: 10.1039/D5LP00189G

(C2) PVA with 2 wt.% β-CD. (d) XRD patterns for PVA/β-CD films. (a-d) Reproduced with permission [64]. © 2023 Wiley-VCH GmbH. (e) Diagram showing the process for making PVA/melamine (MA) films. (f) Stress-strain curves for PVA/MA films. (e,f) Reproduced with permission [65]. © 2013 American Chemical Society. (g) Structures of PVA and four pyrimidine derivatives, including melamine, used as cross-linkers. (h) Tensile curves for PVA and PVA with 1 wt.% of various cross-linkers. (g,h) Reproduced with permission [56]. © 2015 American Chemical Society. (i) Diagram depicting multiple hydrogen bonding between (N,N′ ,N″ -tris(2-aminoethyl)phosphoric triamide (TE)) and PVA. (j) ^{1}H NMR spectra for TE, PVA, and TE/PVA. (k) Stress-strain curves for PVA and TE/PVA. (i-k) Reproduced with permission [69]. © 2021 American Chemical Society. (l) Diagram for the preparation of PVA/ inositol (IN) films. (m) Stress-strain curves for PVA/IN films. (n) IR shift observed in PVA/IN films. (o) In situ IR spectra for (O1) PVA and (O2) PVA with 1 wt.% IN. (l-o) Reproduced with permission [70]. © 2021 American Chemical Society.

Song et al. [65] added melamine (MA) to PVA to design polymeric materials with enhanced mechanical properties via H-bonded interactions (Figure 3e). They demonstrated that the yield strength, Young's modulus, strain at failure, and toughness increased significantly with the addition of 1 wt.% MA. These values reached approximately 72 MPa, 3 GPa, 110%, and 82 MJ/m³, respectively, which represent increases of 22%, 25%, 144%, and 200% compared to those of PVA (see Figure 3f). In addition, the study confirmed the H-bonding interactions between the component through IR spectroscopy and rheological studies. Song et al. [56], in another study, demonstrated how four pyrimidine-derived multiamines, including melamine, and small organic cross-linkers could create strong and tough cross-linked PVA (Figure 3g). The amine groups in each molecule effectively cross-linked PVA through multiple H-bonds. PVA cross-linked with 4N-2456 exhibited significant improvements in yield strength (about 140 MPa), toughness (42 MJ/m³), Young's modulus (3.5 GPa), and strain at break (40%) (Figure 3h). The results from IR spectroscopy, DSC, and rheological tests confirmed the strong hydrogen bonding interactions between the small organic cross-linkers and PVA chains.

By creating multiple hydrogen bonds between (N,N′,N″-tris(2-aminoethyl)phosphoric triamide (TE)) and PVA, Xie et al. [69] aimed to enhance the mechanical capabilities of PVA and develop a dynamic cross-linking structure in conjunction with the hydroxyl-rich structural characteristics of PVA (Figure 3i). The PVA/TE compounds were characterized using ^{1}H nuclear magnetic resonance (NMR) and IR spectroscopy to confirm hydrogen bonding interactions. In the ^{1}H NMR spectra of PVA and PVA/TE, the hydroxyl hydrogen resonance

View Article Online
DOI: 10.1039/D5LP00189G

peak of PVA appeared as a triplet (chemical shifts at 4.23, 4.46, and 4.68) (Figure 3j). These peaks broadened and overlapped to form a single broad peak in the PVA/TE spectrum, indicating hydrogen bonding between PVA and TE. The proton exchange rate slows down during hydrogen bond association, leading to reduced peak intensity and broadening of the resonance peak in the ^{1}H NMR spectra [71–73]. The tensile test results demonstrated that hydrogen bonding improved toughness and strength (Figure 3k). PVA exhibited a tensile strength of 67 MPa, an elastic modulus of 2.7 GPa, and an elongation at break of 267%. With the creation of a hydrogen-bonded cross-linked network, PVA with 5 wt.% TE showed increased strength and modulus (97 MPa and 4.2 GPa), reflecting improvements of 45% and 55%, in turn, and a slight increase in elongation at break to 290%.

Using inositol (IN) molecules as cross-linkers, Xu et al. [70] prepared strong and tough PVA (Figure 3l). The tensile stress-strain curves for PVA/IN are displayed in Figure 3m. The yield strength initially increased and peaked at 1 wt.% IN, reaching 148 MPa, 31% higher than PVA. Although further increases in IN led to a slight reduction in yield strength, it remained higher than that of PVA. The incorporation of IN also caused a brittle-to-ductile transition; the break strain peaked at 86% for 5 wt.% IN, compared to 23% for PVA. Consistent with this trend, the elastic modulus peaked at 2.5 GPa at 1 wt.% IN. Toughness reached around 106 MJ/m³ for 5 wt.% IN, a 5.2-fold increase over PVA. Crucial data about the intermolecular H-bond between PVA and IN was obtained from variable temperature infrared (VTIR) and IR spectroscopy analyses (Figure 3n,o). The addition of IN to PVA caused a noticeable shift in the υ_{O-H} stretching vibration of the hydroxyl groups in the IR spectra. According to the authors, this shift indicated the replacement of stronger PVA-PVA hydrogen bonds with weaker PVA-IN bonds. VTIR measurements further supported these findings, showing a clear blue shift of υ_{O-H} peaks with increasing temperature. This shift showed the dissociation of some H-bonds and the creation of new, weaker hydrogen bonds or free hydroxyl groups in IN. The shifts, which reverted upon cooling, demonstrated that the H-bonds formed between PVA and IN were thermally stable, even at temperatures as high as 150°C [52,74].

View Article Online
DOI: 10.1039/D5LP00189G

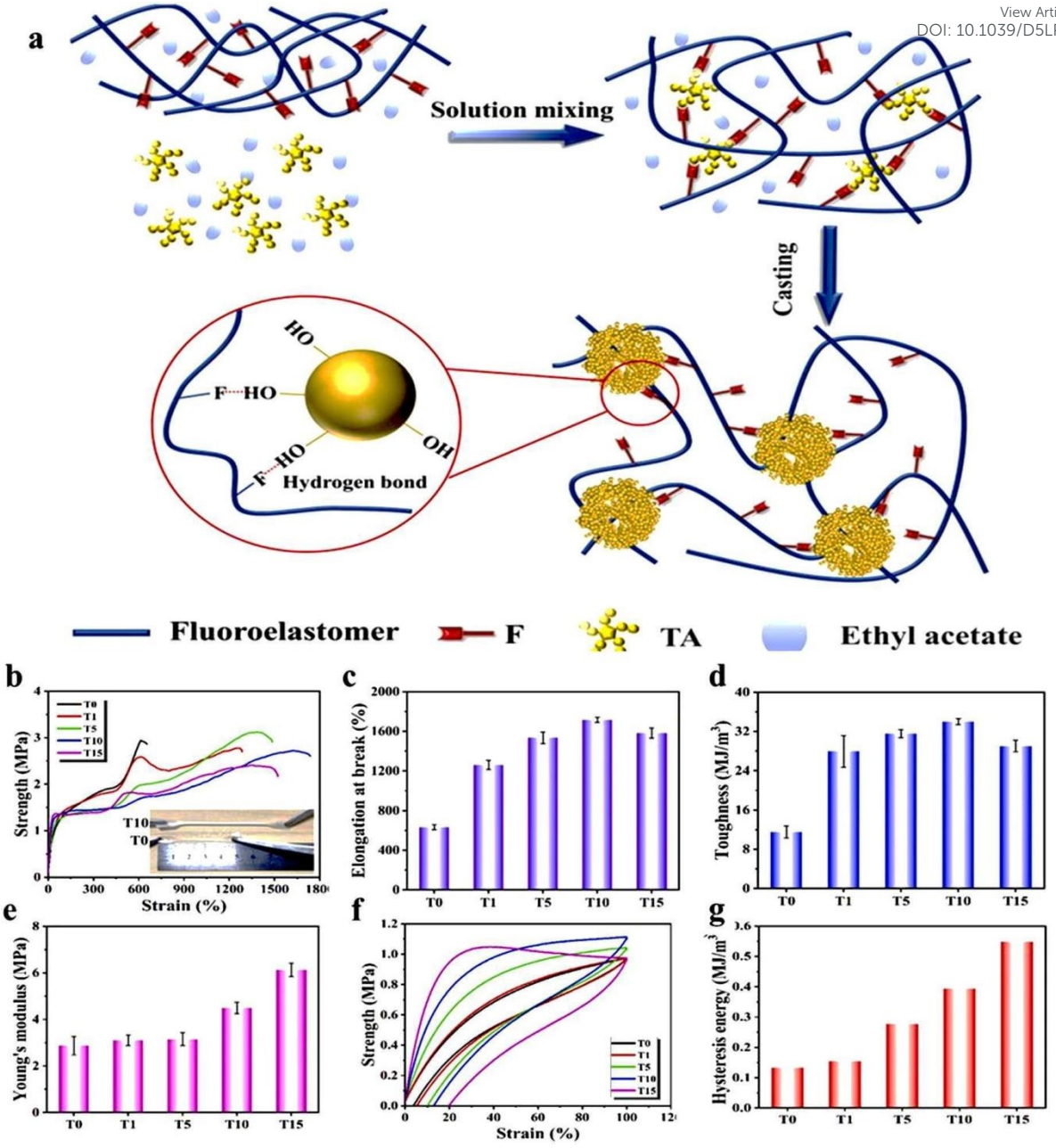

Figure 4. (a) Schematic diagram illustrating the fabrication process of fluoroelastomer/ tannic acid (TA) films. (b) Stress-strain curves (inset shows photographs of fluoroelastomer and fluoroelastomer with 10 wt.% TA during stretching), (c) elongation at break, (d) toughness, (e) modulus, (f) loading-unloading curves, and (g) hysteresis energy for fluoroelastomer, fluoroelastomer with 1, 5, 10, and 15 wt.% TA. (a-g) Reproduced with permission [75]. © 2023 Elsevier B.V. All rights reserved.

By establishing hydrogen bonding with the help of tannic acid (TA), Guo et al. [75] successfully fabricated a stretchable, tough, and stiff fluoroelastomer (FE) (Figure 4a). The mechanical characteristics of the FE were significantly improved by TA (Figures 4b-e). The elongation at

View Article Online
DOI: 10.1039/D5LP00189G

break of the matrix was 634% and increased to a maximum of 1716% at 10 wt.% TA, representing a 171% improvement. The toughness of the system also increased, peaking at 34 MJ/m³ at 10 wt.% TA, approximately three times that of the matrix. Additionally, Young's modulus rose with increasing TA content, reaching a maximum of 6.1 MPa at 15 wt.%, more than twice that of the matrix. The study also included a tensile loading-unloading test at 100% strain, which demonstrated the sacrificial nature of the hydrogen bonds (Figures 4f,g). Each compound exhibited residual strain and notable hysteresis loops in the loading-unloading curves. As the interfacial hydrogen bonds were broken, the hysteresis energy, a measure of energy dissipation, rose with increasing TA content, reaching more than four times the value of FE at 15 wt.% TA. Furthermore, XPS and FTIR spectroscopy were used in this study to confirm the creation of H-bonds in the system.

3.2.The role of nanoparticles

Multiple H-bonding interactions with some polymers can be also facilitated by nanoparticles because of their abundant surface oxygen-containing groups. For example, by uniformly dispersing cellulose nanofiber (CNF) in PVA, Chen et al. [76] fabricated a strong and tough nanocomposite based on H-bonding cross-link sites (Figure 5a). The successful creation of the polymeric materials with hydrogen bond cross-linking was confirmed by DSC, IR spectroscopy, and rheological tests. Tensile testing demonstrated that the tensile characteristics of the compounds were greatly improved by the addition of CNF (Figures 5b,c). PVA showed a tensile stress of 61.8 MPa, a modulus of 3.1 GPa, and a 24.8% elongation at break. These values increased with the addition of 3 wt.% CNF, which had an elongation at break of 129.9%, a tensile stress of 160.7 MPa, and a modulus of 5.1 GPa. The authors claimed that these improvements were facilitated by the potent H-bond interaction between PVA and CNF. Moreover, PVA with 3 wt.% CNF showed remarkable resistance to breaking under load and toughness. The recyclable and healable characteristics of PVA were also retained in PVA/CNF. PVA with 3 wt.% CNF could be dissolved in hot water, filtered, and re-dried for reuse. The nanocomposites only slightly deteriorated after multiple recycling cycles, maintaining good mechanical characteristics (Figure 5d). After seven cycles, there was no discernible loss in ductility and the toughness dropped marginally from 126.3 to 117.2 MJ/m³. The healing properties of recycled PVA/CNF were also analysed by cutting and rejoining the films with water and pressure (Figures 5e,f). Interestingly, without cracking or deforming, the healed film held a 4.5 kg weight. There was less than a 20% loss in the mechanical parameters of the healed film compared to the original, including strength, strain, modulus, and toughness (Figure 5g).

View Article Online
DOI: 10.1039/D5LP00189G

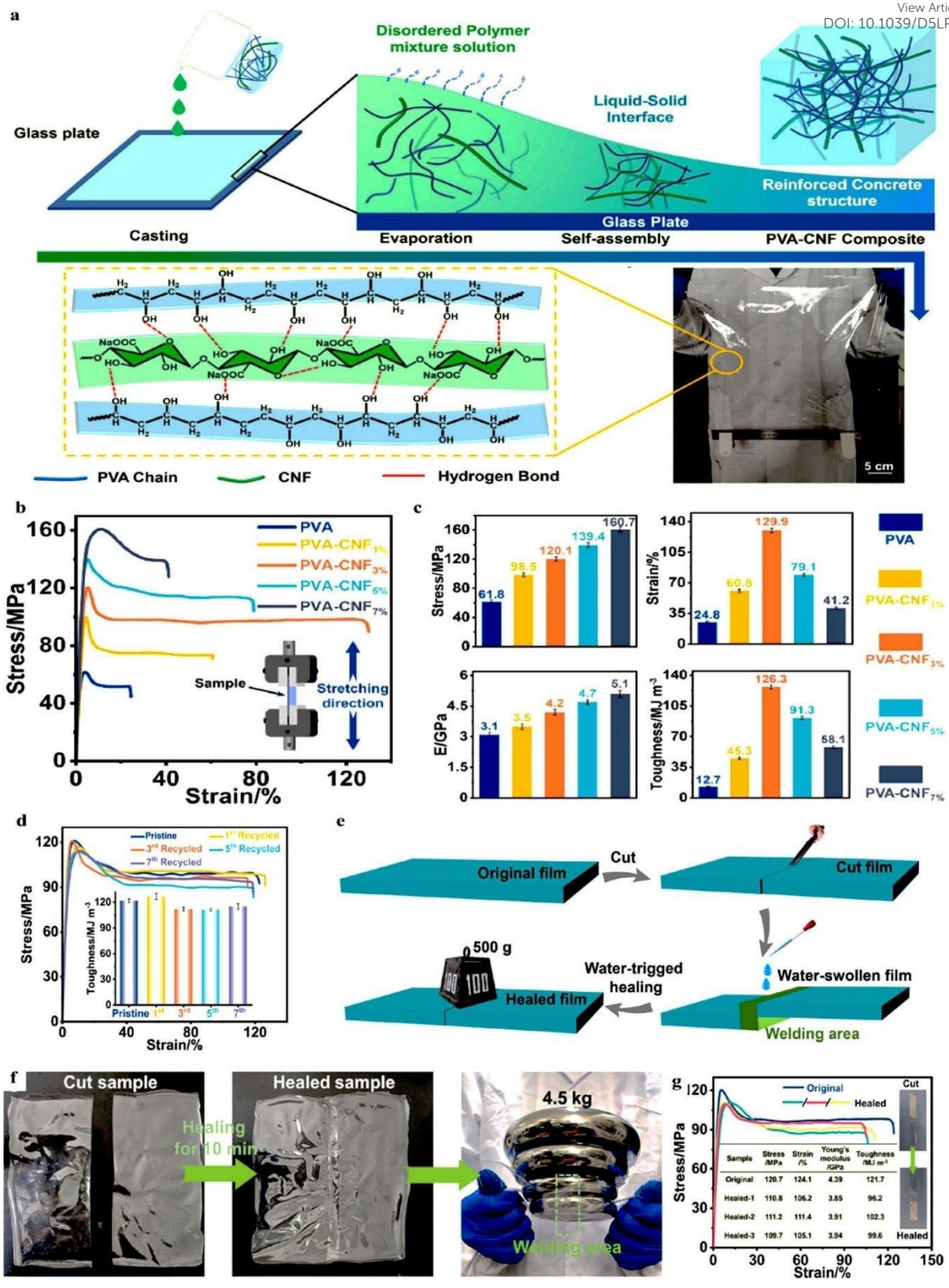

Figure 5. (a) Preparation process of PVA/CNF nanocomposite film and a digital image of the PVA/CNF nanocomposite. (b) Stress-strain curves of PVA and PVA/CNF nanocomposites. (c) Summary of tensile characteristics of PVA and PVA/CNF

View Article Online
DOI: 10.1039/D5LP00189G

nanocomposites. (d) Tensile stress-strain curves of PVA with 3 wt.% CNF before and after diverse recycling cycles. The inset compares the toughness values of pristine and recycled PVA with 3 wt.% CNF. (e) Diagram of the water-assisted healing process for PVA with 3 wt.% CNF. (f) Digital images of cut films before and after healing, showing the healed film (60 μm thick) supporting a 4.5 kg weight. (g) Stress-strain curves of original and healed PVA with 3 wt.% CNF, with an inset displaying cut and healed strips and a table comparing the tensile characteristics of the original and healed strips. (a-g) Reproduced with permission [76].

Song et al. [31] developed graphene oxide dots (GOD) for cross-linking PVA (see Figure 6a). With an abundance of hydroxyl, epoxide, and carboxyl groups on their surface and edges, GOD can crosslink PVA chains and establish multiple H-bonds with PVA due to the abundance of hydroxyl groups in its macromolecules. Tensile tests were conducted to examine the impact of GOD on the tensile characteristics of PVA films reinforced by GOD (Figure 6b). Unlike graphene oxide (GO), the tensile strength and modulus of PVA were improved with GOD without sacrificing ductility. PVA demonstrated a modulus of 2.32 GPa and a yield strength of 91.8 MPa. These were enhanced to 136.3 MPa and 3.76 GPa, respectively, by adding 0.57 vol% GOD, and to 152.5 MPa and 4.35 GPa, by adding 1.16 vol% GOD. Rheological testing indicated a reinforcing effect, with G' of PVA rising approximately linearly with increasing GOD (Figure 6c). At low frequencies, PVA solutions showed a low slope, indicating the creation of a physical cross-linked network. The low-frequency area showed a plateau in G' when GOD surpassed 1 wt.%, suggesting that GOD can efficiently create GOD-centred nanoconfinements by cross-linking PVA chains through multiple hydrogen bonds [56,65,77,78]. Despite having greater G' values, this phenomenon was not seen in GO-reinforced PVA. The plateau in rheological tests was eliminated by fewer H-bond sites of GO and its steric hindrance, disrupting the hydrogen bonds of PVA [79]. For GOD-reinforced PVA, IR spectra showed notable blue shifts in the hydroxyl stretching vibration, indicating strong H-bond interactions (Figure 6d). Conversely, GO-reinforced PVA displayed slight changes due to fewer intermolecular connections and weaker H-bond interactions. Due to strong multiple hydrogen bonding interactions, limiting PVA chain mobility, the T_g of GOD-reinforced PVA also increased with larger GOD content [80,81] (Figure 6e). In contrast, the addition of GO lowered T_g by weakening and isolating the intermolecular hydrogen bonds among the polymeric chains of PVA.

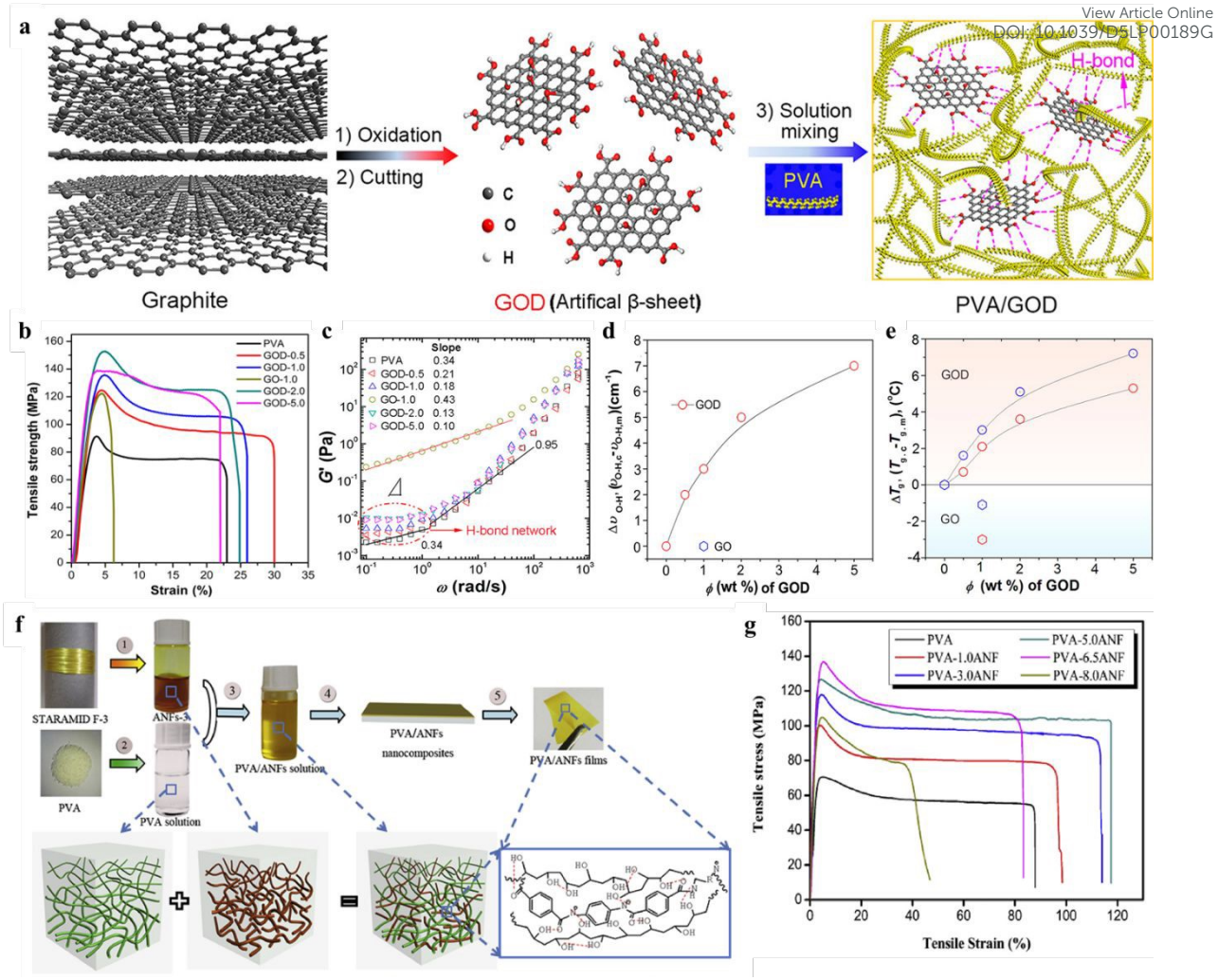

Figure 6. (a) Diagram showing the synthesis of GOD and the process for fabricating PVA/GOD nanocomposites. (b) Tensile curves of PVA and PVA/GOD (c) Frequency dependence of G′ for PVA and PVA/GOD. (d) Wavenumber shift ($\Delta\nu_{O-H}$) and (e) T_g difference (ΔT_g) of PVA and PVA/GOD compared to PVA. (a-e) Reproduced with permission [31]. © 2018 American Chemical Society. (f) Illustration of interactions between PVA and aramid nanofibers (ANFs). (g) Stress-strain curves of PVA and PVA/ANFs. (f,g) Reproduced with permission [82]. © 2017 Published by Elsevier Ltd.

PVA/aramid nanofibers (ANFs) with high strength and toughness were prepared by Guan et al. [82] (Figure 6f). Increasing ANFs improved the tensile strength and modulus of PVA (Figure 6g). This enhancement was because of the efficient stress transfer from PVA to ANFs and strong hydrogen bonding interactions that prevent phase separation. However, excessive ANF loading led to decreased tensile strength due to poor dispersion and stress concentration. In addition, PVA/ANFs exhibited higher elongation at break and toughness, attributed to the disruption and reformation of hydrogen bonds and efficient energy dissipation. To investigate

View Article Online
DOI: 10.1039/D5LP00189G

PVA and ANF hydrogen bonding characteristics, IR analysis and T_g of PVA nanocomposites were also conducted.

Using maleic anhydride-grafted polypropylene (MA-g-PP) and ultrathin two-dimensional (2D) titanium carbide ($Ti_3C_2T_x$) (MXene), Shi et al. [83] fabricated nanocomposites with exceptional mechanical properties (Figure 7a). Results from tensile testing in this study indicated that increased $Ti_3C_2T_x$ loading generally resulted in an improvement in tensile strength (Figure 7b). This improvement was documented because of the hydrogen bonding-created structure, limiting the mobility of the polymer chain and improving tensile characteristics. However, elongation at break was marginally reduced in comparison to PP-g, and the ductility trend differed at low $Ti_3C_2T_x$ loading (< 1 wt.%). On the other hand, elongation at break increased at greater $Ti_3C_2T_x$ levels (> 0.5 wt.%). According to the authors, it could be inferred from this that increased $Ti_3C_2T_x$ loading provided more slippage sites for nanocomposites to be stretched following tensile testing, breaking hydrogen bonds. To comprehend the load transfer and reinforcing mechanism, this work looked at the fractured surfaces of specimens made of PP-g and its nanocomposite (Figure 7c). The fractured surface of PP-g was smooth with micro-voids (Figures 7C1,C'1), but nanocomposites with low $Ti_3C_2T_x$ exhibited a wrinkled morphology with fewer micro-voids and protruding $Ti_3C_2T_x$ thickly coated with polymeric material, indicating strong interfacial adhesion (Figures 7C2-4,C'2-4). An orientated nanosheet structure at 1 wt.% $Ti_3C_2T_x$ suggested slippage at the PP-g/ $Ti_3C_2T_x$ interface (Figure 7C'4). In accordance with the findings of tensile tests, an orientated tearing structure was seen at 2 wt.% $Ti_3C_2T_x$ (Figures 7C5,C'5), indicating the balance between slippage and hydrogen-bonded supramolecular network.

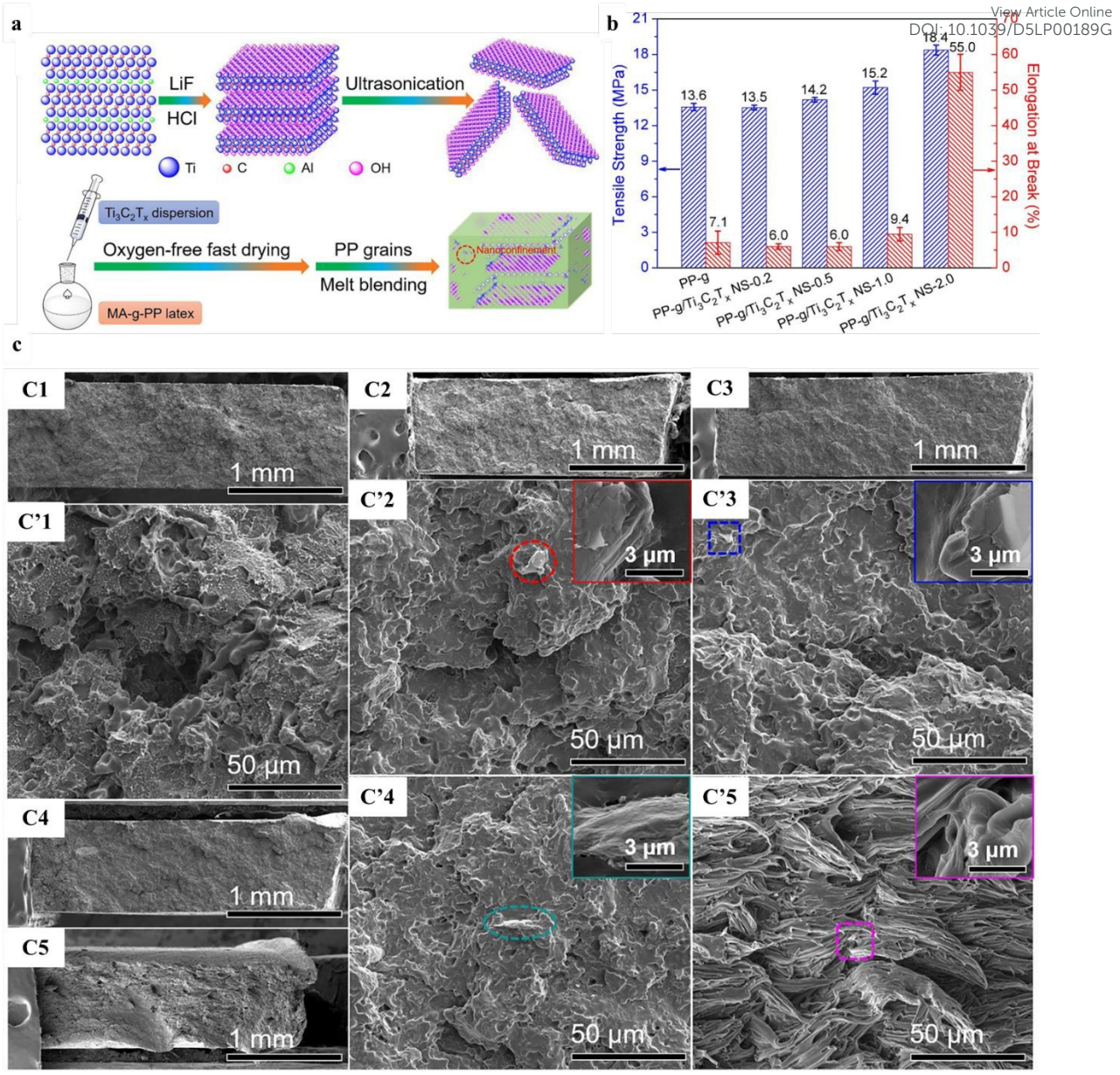

Figure 7. (a) Diagram showing the synthesis of MXene as a hydrogen-bonded cross-linker and the process for fabricating PP-g/ MXene nanocomposites. (b) Tensile properties of PP-g and PP-g/ $Ti_3C_2T_x$. (c) SEM photos of fractured surfaces of (C1, C'1) PP-g, (C2, C'2) PP-g with 0.2 wt.% $Ti_3C_2T_x$, (C3, C'3) PP-g with 0.5 wt.% $Ti_3C_2T_x$, (C4, C'4) PP-g with 1 wt.% $Ti_3C_2T_x$ and (C5, C'5) PP-g with 2 wt.% $Ti_3C_2T_x$. (a-c) Reproduced with permission [83]. © 2019 Elsevier B.V. All rights reserved.

Liu et al. [84] functionalized MXene by *in situ* loading nanoscale zirconium amino-tris-(methylenephosphonate) (Zr-AMP) onto its surface for use in polymer nanocomposites based on thermoplastic polyurethane (TPU) (Figure 8a). They demonstrated that adding functionalized MXene (Zr-MXene) improved the tensile characteristics of TPU (Figure 8b). The TPU exhibited a tensile toughness of 168 MJ/m³, strain at break of 1500%, and tensile

strength of 17.5 MPa. With adding 1 wt.% Zr-MXene, these values increased to 316 MJ/m³ (an 88% boost), 2060% (a 37% rise), and 25.1 MPa (a 43% increase). However, higher Zr-MXene content did not result in further improvements. Cyclic tensile tests were also performed in this study at a fixed strain of 600% to evaluate the anti-fatigue capabilities of TPU/Zr-MXene (Figures 8c,d). Tensile strength declined with the number of fatigue cycles due to the incomplete recovery of broken intermolecular connections before the next cycle. After 100 cycles, TPU retained almost 66% of its initial tensile stress; in contrast, TPU/Zr-MXene with 2 wt.% Zr-MXene retained roughly 71%, indicating superior fatigue resistance. To further understand how H-bond interactions contribute to the enhanced tensile properties of TPU/Zr-MXene, IR spectra of these materials were recorded.

Liu et al. [85], in another study, produced functionalized $Ti_3C_2T_x$ decorated with 10-(2, 5-dihydroxyl phenyl)-9, 10-dihydro-9-oxa-10-phosphaphenanthrene-10-oxide (DOPO-HQ) for the fabrication of TPU nanocomposites (see Figure 8e). They demonstrated how the tensile properties of TPU were affected by the addition of functionalized $Ti_3C_2T_x$ ($Ti_3C_2T_x$-D-H) (Figures 8f-h). It was found that TPU had a tensile strength of 27 MPa and a break strain of 494%. Due to inadequate interfacial adhesion, adding 4 wt.% $Ti_3C_2T_x$ to TPU reduced its tensile strength and break strain. These characteristics were enhanced by adding $Ti_3C_2T_x$-D-H nanohybrid, though. For example, adding 2 wt.% $Ti_3C_2T_x$-D-H improved the tensile strength by 33% to 36 MPa and increased the break strain by 10% to 545.5%. Strong hydrogen bonding with the TPU matrix and the good dispersion of the $Ti_3C_2T_x$-D-H nanohybrid were credited for this improvement. Significant improvements were also made to the toughness of nanocomposites; the TPU with 2 wt.% $Ti_3C_2T_x$-D-H showed a toughness of 90 MJ/m³, a 57% increase. To provide evidence of the hydrogen bonding relationship between the $Ti_3C_2T_x$-D-H nanohybrid and TPU, FTIR analysis was performed on the chemical structure of TPU and its nanocomposites.

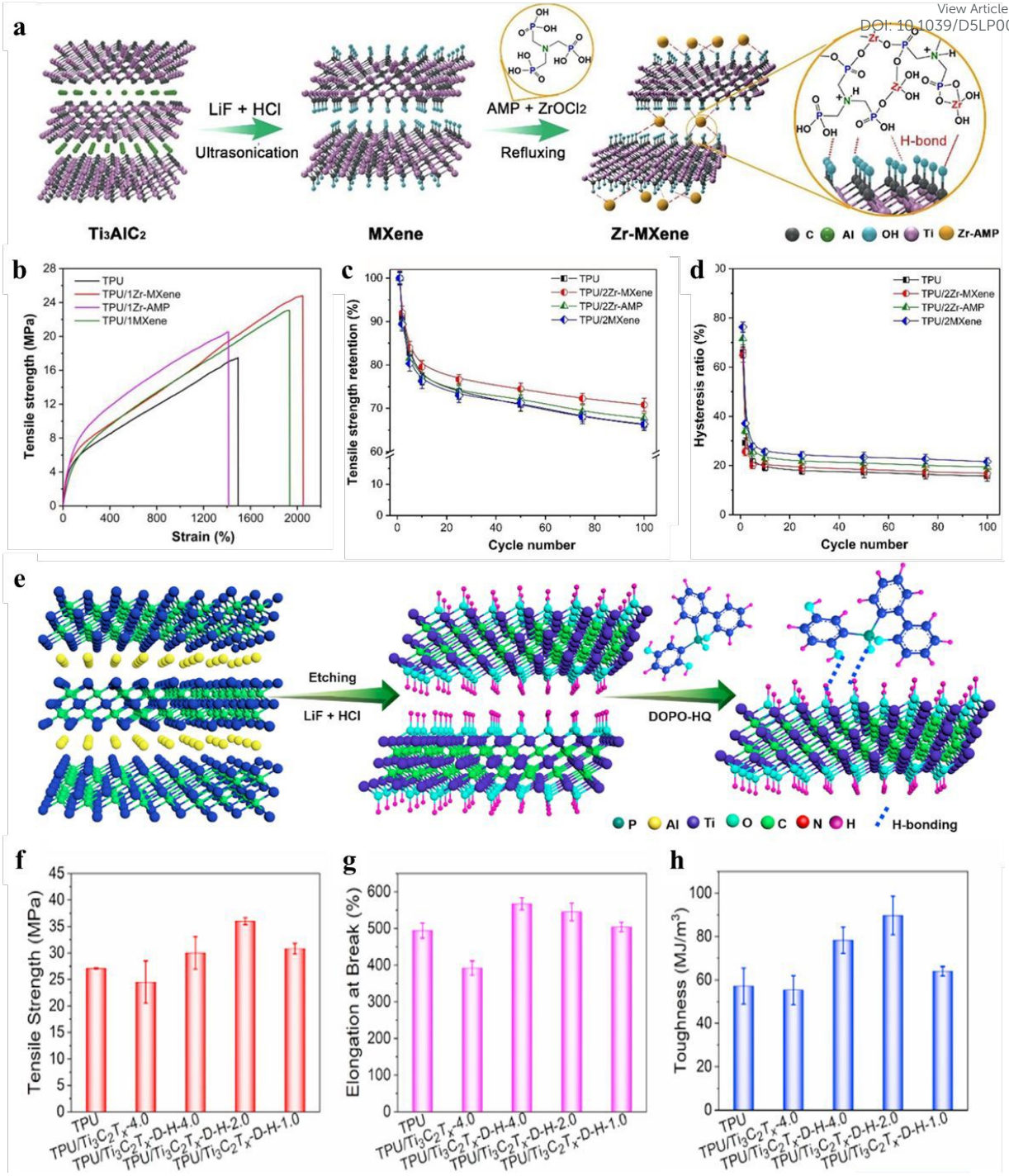

Figure 8. (a) Diagram showing the synthesis of Zr-MXene (b) Representative stress-strain curves, (c) retention of tensile strength, and (d) hysteresis ratio for TPU, TPU/MXene, and TPU/Zr-MXene. (a-d) Reproduced with permission [84]. © 2021 Elsevier B.V. All rights reserved. (e) Illustration for preparation of $Ti_3C_2T_x$-D-H nanohybrid, (f) Tensile strength, (g) elongation at break, and (h) tensile toughness for TPU and TPU/$Ti_3C_2T_x$-D-H. (e-h) Reproduced with permission [85]. © 2022 Elsevier Ltd. All rights reserved.

View Article Online
DOI:10.1039/D5LP00189G

Epoxidized natural rubber (ENR)/organic-modified layered double hydroxide (O-LDH) polymeric materials with improved mechanical properties were prepared by Li et al. [86] (Figure 9a). The stretching peak of O-H groups and the T_g of the nanocomposites confirmed the formation of a hydrogen-bonded supramolecular network in the ENR/O-LDH. Tensile stress, break strain, and elastic modulus rose to 2.80 MPa, 542%, and 4.70 MPa, respectively, when the O-LDH content in the ENR nanocomposite reached 20 phr (Figures 9b–d). These values were 366%, 113%, and 427% of those for ENR. The primary cause of this notable improvement in strength and ductility is the reinforcement provided by O-LDH nanosheets and the creation of a dynamic hydrogen-bonded supramolecular network, which allows greater energy dissipation during loading through quick hydrogen bond breakage and recombination [31,87]. Effective self-healing was also demonstrated by ENR/O-LDH (Figures 9e–h). After 12 hours of healing at 120°C, they became extremely flexible and were able to lift a kilogram of weight. The thermodynamic hydrogen-bonded network and low T_g of ENR, which enable quick chain rearrangement and bond repair, are responsible for the minimal visible damage observed in optical images after healing. Due to limited chain mobility, healing efficiency rose to 10 phr of O-LDH before declining at higher concentrations. The maximum effectiveness of 78% was attained after 12 hours of recovery.

View Article Online
DOI: 10.1039/D5LP00189G

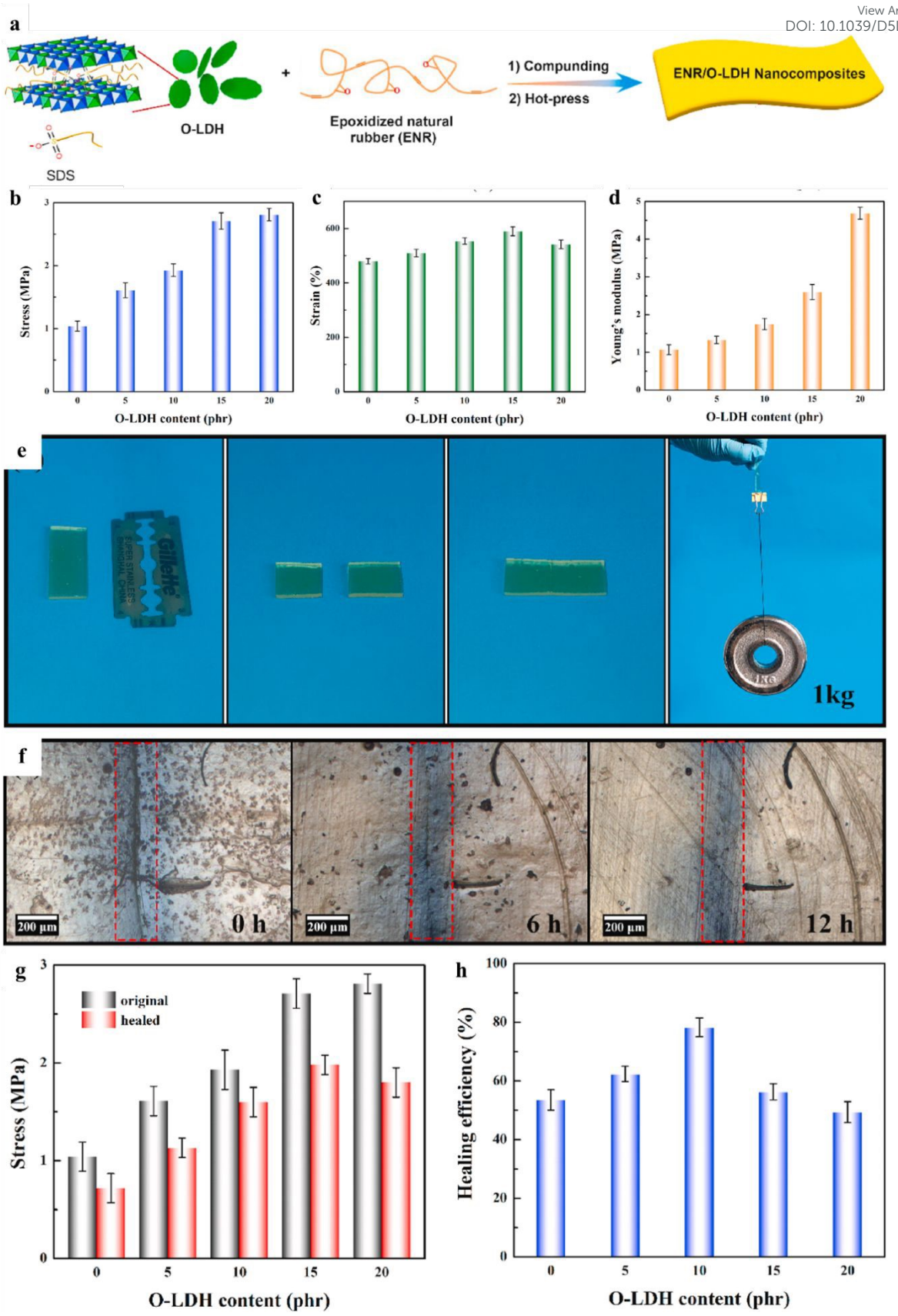

Figure 9. (a) Illustration of the conceptual design of strong, tough and self-healable ENR/O-LDH nanocomposites, (b) Stress, (c) strain, and (d) Young's modulus for ENR/O-LDH. (e)

Images of ENR with 10 phr O-LDH following self-healing at 120°C for 12 hours. (f) Optical microscope images of ENR with 10 phr O-LDH before healing, after 6 hours of healing at 120°C, and after 12 hours. (g) Stress and (h) healing efficiency for ENR/O-LDH. (a-h) Reproduced with permission [86]. © 2020 Elsevier Ltd. All rights reserved.

Graphene nanodots (GNDs) were used by Fang et al. [88] to manufacture strong and tough poly(ε-caprolactone) (PCL) nanocomposites (Figures 10a,b). To examine the intermolecular hydrogen bonding interactions between PCL and GNDs, FTIR and XPS tests were performed on the PCL nanocomposites. The tensile stress-strain behaviour of GNDs/PCL revealed that tensile strength and break strain initially increased with GND loading, then marginally decreased (Figures 10c-e). Tensile strength increased to 27 MPa (a 46% increase over PCL) at 1 wt.% GNDs and to 34 MPa (an 82% increase) at 2 wt.% GNDs, before slightly decreasing to 23.8 MPa, which was still higher than PCL. The break strain also rose, peaking at 674% at 2 wt.% GNDs, which was 46% better than PCL. Similar trends were observed in toughness and elastic modulus, with toughness reaching a maximum of 134 MJ/m³ and the elastic modulus reaching a maximum of 380 MPa at 2 wt.% GNDs (a 46% increase). SEM examination of fracture morphologies and the high mechanical performance of GNDs/PCL showed a matrix deformation structure and H-bond cross-linking network compared to PCL (Figures 10f-h). A visible 3D H-bond cross-linking network at the fracture interface and the pull-out of PCL chains were outcomes of the potent nanoconfinement phase around GNDs caused by multiscale H-bond interactions [89]. These multiple H-bond networks caused matrix deformation, crack deflection, and crack tearing, enhancing the strength, ductility, modulus, and toughness of GNDs/PCL.

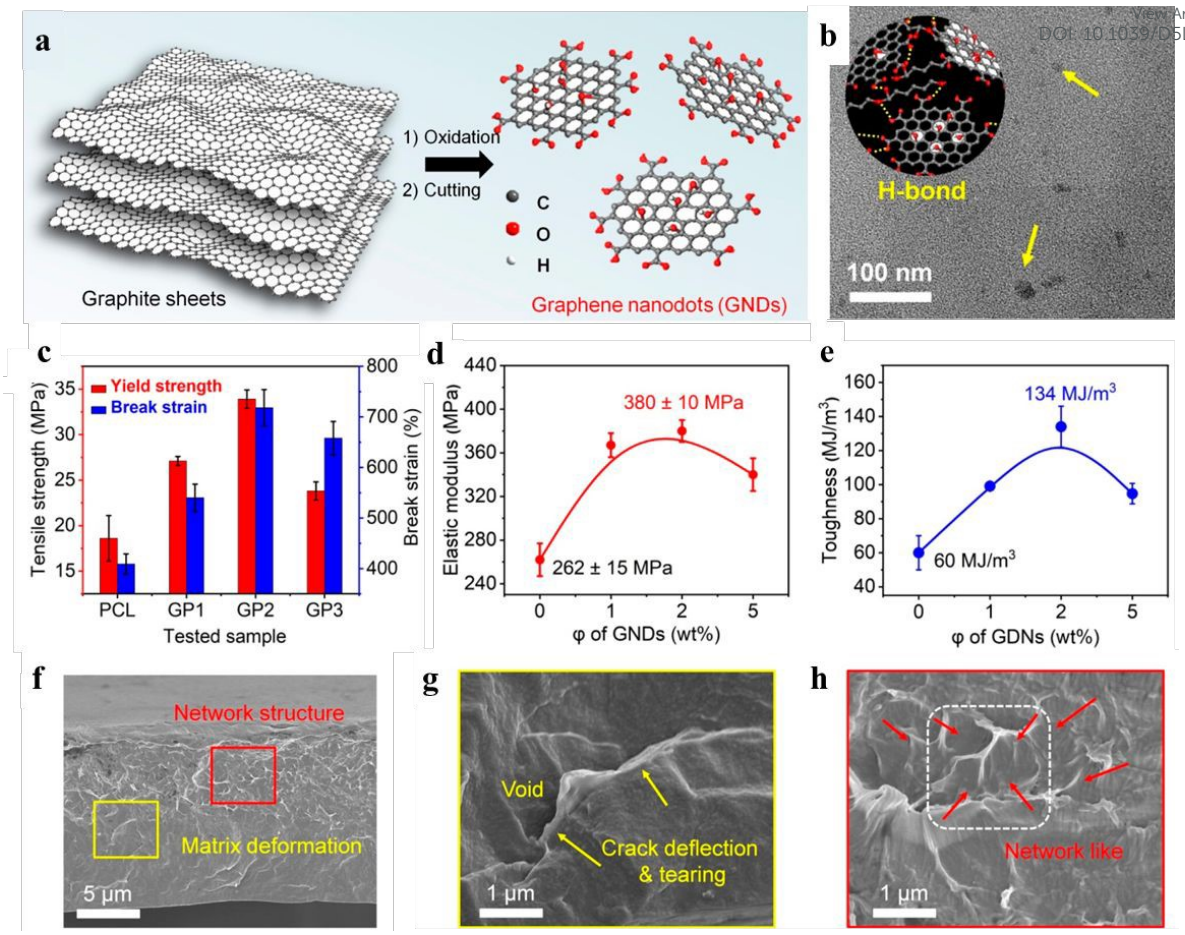

Figure 10. (a) Diagram showing the synthesis of GOD, (b) The cross-sectional transmission electron microscopy (TEM) image of PCL/GOD nanocomposite, (c) Tensile strength and breaking strain, (d) elastic modulus, and (e) tensile toughness for poly(ε-caprolactone) (PCL) and PCL/Graphene nanodots (GNDs). (f-h) SEM photos displaying the fracture morphology of PCL with 2 wt.% GNDs. (a-h) Reproduced with permission [88]. © 2023 American Chemical Society.

3.3.The role of polymer aggregates

Multiple hydrogen-bonded cross-linked polymers can function as efficient cross-linkers for other polymers. For instance, Song et al. [90] developed PVA/sulfonated styrene–ethylene/butylene–styrene triblock copolymer (SSEBS) films where sulfonate groups in SSEBS interacted with hydroxyl groups in PVA to form an H-bonded polymer network through multiple hydrogen bonding, as shown in Figure 11a-d. These interactions were confirmed by rheological data. Tensile strength and breaking strain rose simultaneously when a small quantity of SSEBS was added, as shown in Figure 11e, due to strong hydrogen bonds and the evenly distributed SSEBS inside PVA (see Figures 11b-d). Increasing 10 wt.% SSEBS, the H-bonding allowed the strain at break of PVA to improve from about 30% to 205% without

sacrificing strength, resulting in a toughness of 122 J g^{-1}. However, because of the reinforcing and plasticizing effects of SSEBS, adding more SSEBS rapidly reduced strength and extensibility.

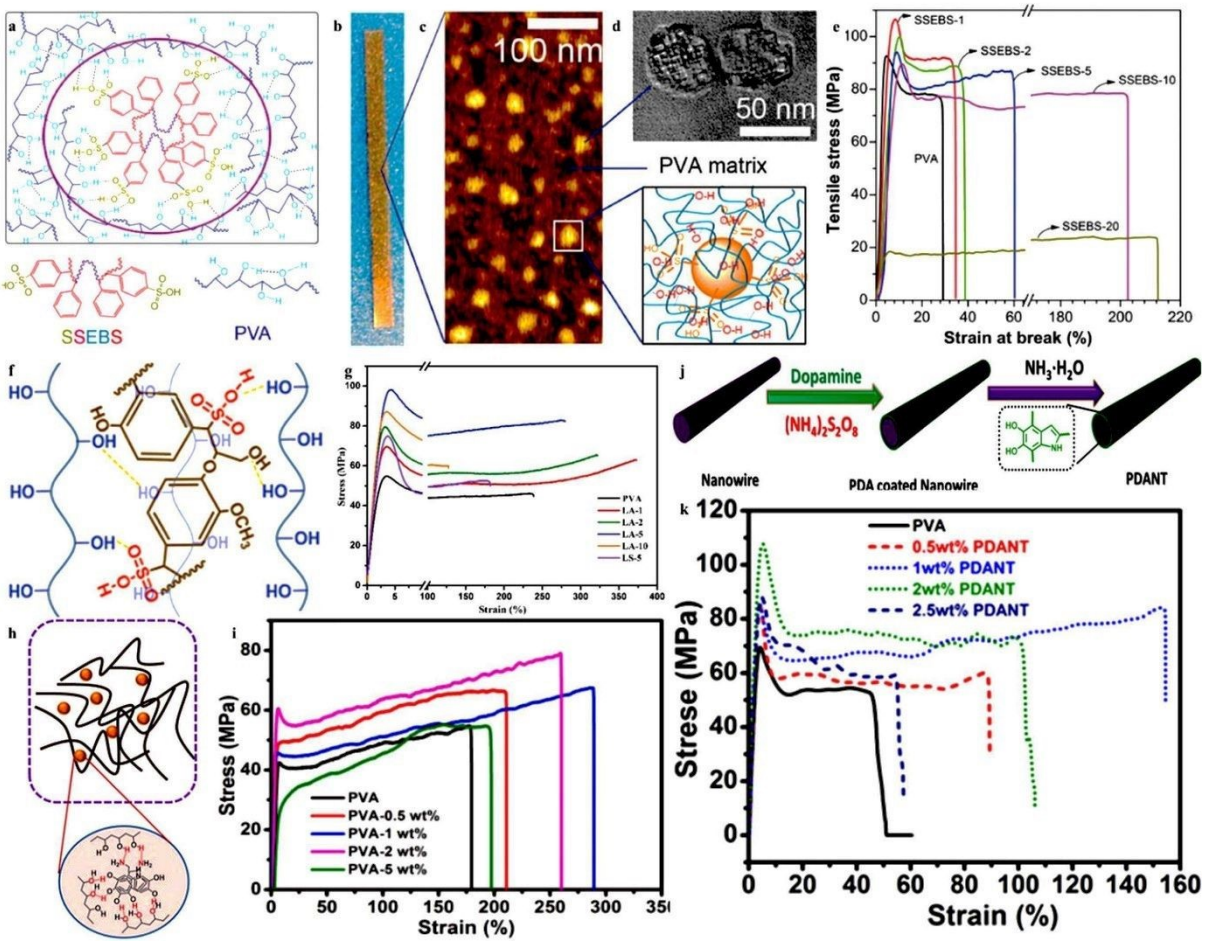

Figure 11. (a) Diagram showing the formation of multiple hydrogen bonds among PVA and SSEBS. (b-d) Digital and atomic force microscopy (AFM) images of PVA containing 10 wt.% evenly distributed SSEBS, along with a TEM image illustrating the self-assembly of SSEBS into phase-separated domains. (e) Stress-strain curves for PVA and PVA/SSEBS. (a-e) Reproduced with permission [90]. © 2017 WILEY-VCH Verlag GmbH & Co. KGaA, Weinheim. (f) Diagram depicting the hydrogen bonds in PVA/ biomass-derived lignosulfonic acid (LA). (g) Stress-strain curves for PVA/LA. (f,g) Reproduced with permission [51]. © 2018 WILEY-VCH Verlag GmbH & Co. KGaA, Weinheim (h) Diagram showing the creation of multiple H-bonds between PVA and polydopamine (PDA). (i) Representative tensile curves for PDA/PVA. (h,i) Reproduced with permission [91]. © 2021 Elsevier Ltd. All rights reserved. (j) Overview of the fabrication process for polydopamine nanotube (PDANT). (k) Representative stress-strain curves for PVA and PDANT/PVA. (j,k) Reproduced with permission [92]. © 2020 Elsevier Ltd. All rights reserved.

View Article Online
DOI: 10.1039/D5LP00189G

Zhang et al. [51] prepared polymeric materials by adding biomass-derived lignosulfonic acid (LA) into PVA (Figure 11f). The tensile behaviour of PVA/LA was studied, showing significant enhancements in strength, modulus, and toughness compared to PVA (Figure 11g). The elongation at break was improved from 238% to 361% with only a 1 wt.% addition of LA; however, it rapidly decreased with increasing LA. With 5 wt.% LA, the tensile strength and modulus were enhanced by 79% and 90% over PVA, in turn, to their highest values of 98.2 MPa and 3.37 GPa. The authors found that the stiff 3D molecular structure of LA and a robust H-bonded network correlated with the greatest mechanical performance in PVA with 5 wt.% LA. IR spectra and rheological studies were utilized to determine H-bond interactions between PVA and LA.

Strong and tough PVA containing polydopamine (PDA) were fabricated by Xiong et al. [91] (Figure 11h). Figure 11i illustrates the tensile behaviour, such as tensile strength and modulus, elongation at break, and toughness. Stress-strain curves for PVA with less than 2 wt.% PDA was comparable to those of PVA, demonstrating a yield at low strain followed by strain hardening. However, the yielding stage vanished at 5 wt.% PDA, showing a notable alteration in the PVA characteristics. PVA showed an elongation at break of 168%, a toughness of 83 MJ/m³, a tensile strength of 54 MPa, and a modulus of 1.67 GPa. These characteristics improved with less than 2 wt.% PDA; for example, PVA with 2 wt.% PDA demonstrated improvements of 43% and 66%, respectively, in tensile strength (77 MPa) and tensile modulus (2.77 GPa). Its elongation at break and toughness were also improved by nearly 55% and 105%, reaching 260% and 170 MJ/m³. However, at 5 wt.% PDA, mechanical properties declined due to the increase of amorphous PVA. Evidence for the development of an H-bonding cross-linking network came from IR measurements and rheological experiments.

Fang et al. [92] prepared polydopamine nanotube (PDANT)/PVA with improved mechanical properties using a simple solution-casting method. In this work, ammonium molybdate nanowire was utilized as a template to synthesize PDANT inspired by mussels (Figure 11j). Through tensile testing, the mechanical characteristics of PDANT/PVA were assessed (Figure 11k). PVA exhibited a modulus of 3 GPa and a strength of 67 MPa. The addition of PDANT resulted in improvements of approximately 63% and 34%, respectively, in strength and modulus up to an ideal content of 2 wt.%, where the strength reached 109 MPa and the modulus 4.01 GPa. The authors ascribed this improvement to hydrogen bonds between PDANT and the matrix, enhanced crystallinity, and the higher mechanical qualities of cross-linked polydopamine. The breaking strain and toughness of PDANT/PVA also improved

View Article Online
DOI: 10.1039/D5LP00189G

dramatically. For instance, PVA containing 1 wt.% PDANT demonstrated a toughness of 1102 MJ/m³ and an ultimate strain of 122%, which were increases of 144% and 324%, respectively, over PVA. IR spectra confirmed the H-bond interactions between PDANT and PVA chains.

4. Comparative analysis of particle-based cross-linkers and multiscale hydrogen-bond synergy

Direct comparison of the tensile properties of reported multiple hydrogen-bonded polymer networks is challenging. This complexity arises from variations in polymer matrices, cross-linker chemistry, filler loadings, processing conditions, mechanical testing protocols, and other factors. To address these inconsistencies, we calculated the percentage improvement in strength, modulus, strain at break, and toughness compared to the neat polymer for each study. This approach gives us a more meaningful evaluation of the trends across various types of cross-linkers. Table 1 displays the values and associated percentage improvements for the studies examined in this work.

Table 1 shows that small molecules often perform exceptionally well in increasing strain at break and toughness, presumably due to their greater mobility in the polymer matrix, even though they typically provide only moderate reinforcement in strength and modulus. However, in most cases, nanoparticles produce the largest improvements in modulus and strength, attributed to their high aspect ratio, large surface area, and rigid nature. While nanoparticles offer moderate improvements in strain at break and toughness, often lower than those achieved with small molecules, exceptional cases, such as PVA/CNF, exhibit high performance across all properties. Polymer aggregates tend to give balanced improvements in strength, modulus, strain at break, and toughness, although some systems, like PVA/SSEBS, differ from this trend.

View Article Online
DOI: 10.1039/D5LP00189G

Table 1. Tensile properties and corresponding percentage improvements (Δ) of multiple hydrogen-bonded polymer networks incorporating various particle-based cross-linkers, as reported in the studies reviewed in this work.

Cross-linker	Loading	Strength (MPa)(Δ)	Modulus (GPa)(Δ)	Strain at break (%)(Δ)	Toughness ($MJ \cdot m^{-3}$)(Δ)	Ref.
PVA/HCPA	0-10 wt.%	90-147 (+63%)	2.1-3.21 (+53%)	36-101 (180%)	24-112 (+367%)	50
PVA/β-CD	0-10 wt.%	113-136.5 (+21%)	2-3 (+50%)	22.5-112 (+398%)	20.3-118 (+481%)	64
PVA/MA	0-5 wt.%	53.9-65 (+21%)	2.32-2.91 (+25%)	45-109.8 (+144%)	22-66 (+200%)	65
PVA/4N-2456	0-5 wt.%	97-138 (+42%)	2.4-3.5 (+46%)	20-40 (+100%)	17-42 (+147%)	56
PVA/TE	0-20 wt.%	67-97 (+45%)	2.7-4.2 (+55%)	267-290 (+8%)	NA	69
PVA/IN	0-10 wt.%	113-148 (+31%)	2-2.5 (+25%)	23-86 (+274%)	20.3-106 (+422%)	70
FE/TA	0-15 wt.%	NA	0.003-0.004 (+50%)	634-1716 (+171%)	11.5-34 (+196%)	75
PVA/CNF	0-7 wt.%	61.8-160.7 (+73%)	3.1-5.1 (+64%)	24.8-129.9 (+424%)	12.7-126.3 (+894%)	76
PVA/GOD	0-5 vol.%	91.8-152.5 (+66%)	2.32-5.08 (+119%)	23-30 (+30%)	16.8-30.3 (+80%)	31
PVA/ANF	0-8 wt.%	70.6-136.6 (+93%)	4.4-5.2 (+18%)	87.9-117.7 (34%)	50.2-124.9 (+148%)	82
PP-g/MXene	0-2 wt.%	13.6-18.4 (+35%)	NA	7.1-55 (+675%)	NA	83
ENR/O-LDH	0-20 phr	1.04-2.81 (+170%)	0.001-0.005 (+400%)	480-542 (+13%)	NA	84
TPU/Zr-MXene	0-2 wt.%	17.5-25.1 (+43%)	0.011-0.017 (+54%)	1500-2060 (+37%)	168-316 (+88%)	86
TPU/MXene-D-H	0-4 wt.%	27.1-36 (+33%)	NA	494.3-545.5 (+10%)	57.2-89.7 (+57%)	87
PCL/GND	0-3 wt.%	18.6-33.9 (+82%)	0.262-0.38 (+46%)	461-674 (+46%)	60-134 (+123%)	88
PVA/SSEBS	0-20 wt.%	91.2-92.3 (-1%)	1.85-2.41 (-23%)	30-205 (+583%)	17.4-122 (+601%)	90
PVA/LA	0-10 wt.%	54.8-98.2 (+79%)	2.3-3.37 (+46%)	238-282 (+18%)	105.9-219.2 (+107%)	51
PVA/PDA	0-5 wt.%	54-77 (+43%)	1.67-2.77 (+65%)	168-260 (+56%)	83-170.1 (+105%)	91
PVA/PDANT	0-2.5 wt.%	67-109 (+62%)	3-4.01 (+34%)	50-100 (+100%)	26-78 (+200%)	92

While the earlier comparison can provide some indication of the individual roles of small molecules, nanoparticles, and polymer-aggregates, their combined effects across different length scales are equally important. Small molecules operate at the molecular scale to make hydrogen bond switching rapid and reversible, thereby improving toughness and ductility [93]. Nanoparticles, which are found in the nano- to sub-micrometer range, provide high stiffness and strength due to their rigid load-bearing frameworks [94,95]. At the microscale, hydrogen

View Article Online
DOI: 10.1039/D5LP00189G

bonding and physical entanglement work together to give polymer aggregates long-term stability and balanced reinforcing [96]. This indicates that using cross-linkers from various scales can lead to synergistic effects. Such multiscale architectures could enable the simultaneous improvement of strength, stiffness, stretchability, and toughness. A notable example is the dynamic nanoconfinement quenching strategy reported by Zhao et al. [97], in which tannic acid, cellulose nanocrystals, and a PVA matrix achieved exceptional improvements over pure PVA in tensile strength (~170%), modulus (~120%), strain at break (~200%), and toughness (~550%). This demonstrates the potential of multiscale synergy to surpass the performance of any single cross-linker type.

5. H-bond metrics and structure–property relationships

As discussed, hydrogen-bonded cross-linked polymers offer a unique ability for mechanical behavior modification. Two of the significant quantitative metrics that serve as vital links between macroscopic features and molecular-scale interactions are bond strength/energy and bond lifetime/kinetics. The interplay between these two metrics governs the structure–property relationships of H-bond cross-linked polymers.

By decreasing chain slippage under stress, stronger hydrogen bonds or multiple H-bonds can withstand greater loads before dissociating, improving tensile strength and stiffness [98]. The polymer may behave more like a highly cross-linked network, which can be brittle if there are too many or too strong bonds [99,100]. According to an experiment, modulus typically increases as the concentration of H-bonding units in elastomers increases; however, above a critical concentration, extensibility is sacrificed to achieve the increased stiffness [101]. Bonds that are both strong enough to support the network and weak enough to break under load in a controlled way typically exhibit optimal performance.

The lifetime of a hydrogen bond, or how long it typically lasts before dissociating, is another controlling parameter of the time-dependent mechanical properties of H-bond cross-linked polymers. When these bonds have short lifetimes, they can break and reform quickly, which enhances the material's extensibility and toughness by allowing the chains to shift and absorb energy. On the other hand, longer lifetimes make these H-bond cross-links function almost like permanent connections in the short term. This stability enables the material to withstand stress better, resulting in increased stiffness and strength, while also slowing down stress relaxation [102]. An ideal balance often arises when the bond lifetime is comparable to the stress relaxation

View Article Online
DOI: 10.1039/D5LP00189G

time of the polymer because bonds remain intact under rapid loading but gradually dissociate during slower deformation, maximizing toughness while preventing brittle failure [103].

In many cases, optimum performance derives from a synergistic combination of these extremes, obtaining the requisite rigidity together with controlled energy dissipation [104,105]. These are the bases for rational polymeric material design specific to the mechanical and functional requirements of specific applications.

6. Applications of polymeric materials with exceptional performance via multiple hydrogen-bonded networks

A multitude of technological applications depend on the development of new materials with strong mechanical and self-healing properties. Because of their reversible and dynamic interactions, supramolecular polymers, especially those cross-linked by hydrogen bonds, have become attractive options. These materials exhibit remarkable extensibility, toughness, and strength, making them suitable for a variety of applications.

In the field of biomedicine, for example, hydrogen bonds are essential because they affect the bioactivity and biocompatibility of polymeric materials. Hydrogen bonds promote cell adhesion, proliferation, and differentiation in bone scaffolds by improving the interaction between the scaffold and the surrounding biological environment [106,107]. The biocompatibility of PVA/HCPE was evaluated for their potential use as artificial ligaments by Liu et al. [67]. Human umbilical vein endothelial cells (HUVECs) cultured on the PVA and PVA/HCPE films for 72 hours showed similar morphologies to the control group, indicating normal cell metabolism (Figures 12a,b). Fluorescence images confirmed the high viability of HUVECs on the PVA/HCPE films, with cell viability greater after seven days than that of PVA and like the control group.

Beyond biomedical uses, multiple hydrogen-bonded networks have been integrated into advanced sensing devices. Utilizing supramolecular multiple H-bonding polymers (MHBP), an extremely responsive and self-repairing sensor for human-machine interaction (HMI) was developed [108] (Figure 12c). This sensor combined MHBP with a carbon nanotube conducting network in chitosan-decorated epoxy natural rubber latex to establish multiple H-bonds with carboxyl cellulose nanocrystals. The HMI system showed promise for robotic patient support when it was combined with signal-processing software to identify speech and facial expressions.

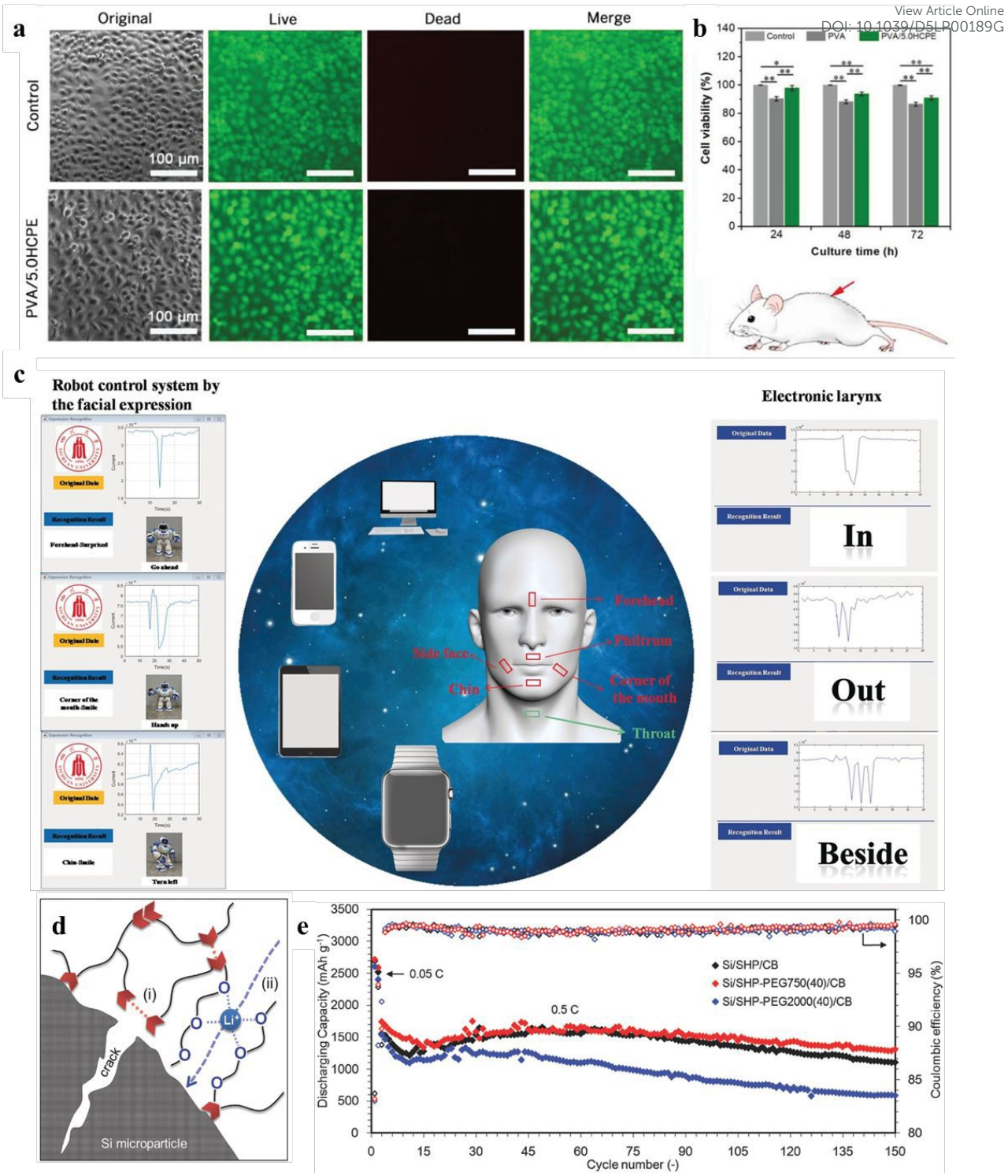

Figure 12. (a) Fluorescent photos from a live/dead assay depicting HUVECs cultured on PVA/HCPE for a duration of 72 hours. (b) Evaluation of cell toxicity in polymeric films after culturing HUVECs for 24, 48, and 72 hours. (a,b) Reproduced with permission [67]. © 2021 Wiley-VCH GmbH. (c) Human-machine interaction system showcasing facial expression (left) and speech (right) detection using strain sensors made from supramolecular multiple hydrogen-bonded network elastomer and signal processing software. Reproduced with

View Article Online
DOI: 10.1039/D5LP00189G

permission [108]. © 2017 Wiley-VCH Verlag GmbH & Co. KGaA, Weinheim. (d) A self-healing polymeric (SHP–PEG) binder, engineered with optimized viscoelasticity and stretchability through multiple hydrogen bonding interactions, designed to preserve the structural integrity of Si electrodes throughout charge–discharge cycling. (e) Cycle performance and coulombic efficiency of Si electrodes with different PEG binders. (d,e) Reproduced with permission [109]. © 2018 WILEY-VCH Verlag GmbH & Co. KGaA, Weinheim.

Bao et al. [109] reported another intriguing application of self-healing H-bonded cross-linked polymeric materials by incorporating poly (ethylene glycol) (PEG) as binders into silicon anode electrodes (Figure 12d). Through multiple H-bond interactions, the self-healing ability of PEG efficiently preserved the integrity of the interface between silicon nanoparticles and electrolytes by optimizing the chemical structure. The resulting lithium-ion battery showed a good discharge capacity of 2600 mAh/g and good cyclic properties (Figure 12e). After the H-bonded binder film was scraped and left to repair at ambient temperature, excellent self-healing was seen, as well. The approach shows promise for future high-capacity batteries experiencing significant volume changes or damage during cycling.

Adoption of exclusively hydrogen-bonded cross-linked networks on an industrial scale remains rare, despite strong research interest. The Cartiva® Synthetic Cartilage Implant, which was approved by the U.S. Food and Drug Administration (FDA) to treat osteoarthritis in the first metatarsophalangeal joint, is among the most prominent biomedical uses [110]. Physically crosslinked PVA hydrogels are used to create this implant, and repeated freeze-thaw cycles promote the development of hydrogen-bonded crystallite domains [111]. The implant has long-term *in vivo* stability, cartilage-like viscoelasticity, and adjustable mechanical qualities thanks to these reversible physical crosslinks.

In the industrial sector, hot-melt adhesives represent one of the most widespread uses of multiple hydrogen-bonded polymer networks. Such adhesives are generally employed in electronics, filtration, automotive, and aerospace manufacturing. For example, Henkel's TECHNOMELT® PA line of polyamide-based hot-melt adhesives offers high strength, flexibility, and chemical and heat resistance, with strong inter-chain hydrogen bonds (https://www.henkel-adhesives.com/au/en/products/industrial-adhesives/hot-melt-adhesives.html). Arkema's Reverlink™, a self-healing elastomer with reversible intermolecular interactions, is another commercial example (https://www.arkema.com/global/en/media/newslist/news/global/innovation/2009/20090527-

View Article Online
DOI: 10.1039/D5LP00189G

self-healing-elas/). This material features a three-dimensional network of small molecules and oligomers with multi-site hydrogen bonding interactions at both terminal and backbone sites [112,113]. The reversible nature of H-bonds allows the material to recover nearly all of its original strength after being cut or scratched under gentle pressure at room temperature without the need for healing agents or external stimuli.

7. Conclusions and outlook

Recently, hydrogen-bonded cross-linking has been widely utilized to tailor the mechanical properties of polymeric materials. The reversible nature of hydrogen-bonded cross-linking enables these materials to exhibit unique mechanical behaviour and self-healing capability. Relatively, different hydrogen bonds are easy to create via a range of approaches such as adding particle-based cross-linkers. This approach enables precise tuning of mechanical performance, making these materials suitable for demanding applications.

Hydrogen-bonded networks have inherent drawbacks despite their benefits. One major issue is that hydrogen bonds can easily be disrupted by moisture, which can gradually weaken their mechanical strength, especially in humid conditions [114]. While it might seem like a downside at first, the sensitivity to moisture has been utilized to develop water-responsive materials. These materials can trigger self-healing and adapt their mechanical properties in a controlled way [115,116]. Moreover, this type of polymeric material often displays hysteresis under cyclic tensile loading because the reformation of disrupted hydrogen bonds takes a certain amount of time [117]. Nonetheless, this hysteresis can be beneficial, as it aids in dissipating fracture energy during deformation, thereby contributing to improved fracture toughness. These aspects must be carefully considered and, where possible, used in the design of next-generation high-performance polymeric materials.

Looking ahead, the field of multi-hydrogen-bonded polymer networks has a great deal of scope for revolutionary advances along several novel research directions, as schematically illustrated in Figure 13. For example, by taking inspiration from nature, such as the hierarchical designs of nacre that incorporate multiple hydrogen bonds, multi-scale energy dissipation pathways that achieve a remarkable balance between toughness and strength can be designed. Another fascinating direction is the development of stimuli-responsive systems, which adapt to various external stimuli, not just humidity, to offer accurate, on-demand control for smart applications. Multifunctional particle-based cross-linkers can increase their potential uses by enhancing mechanical strength, self-healing, and other characteristics like conductivity, biodegradability,

View Article Online
DOI: 10.1039/D5LP00189G

or bioactivity. Computational design technologies such as machine learning, molecular dynamics, and density functional theory can speed up these developments, as well. Beyond their current and emerging uses, these high-performance polymeric materials hold great promise for entirely new and revolutionary applications. To bridge the gap between laboratory prototypes and large-scale commercial production, future efforts should concentrate on scalable and cost-effective fabrication techniques from an industrial and manufacturing perspective.

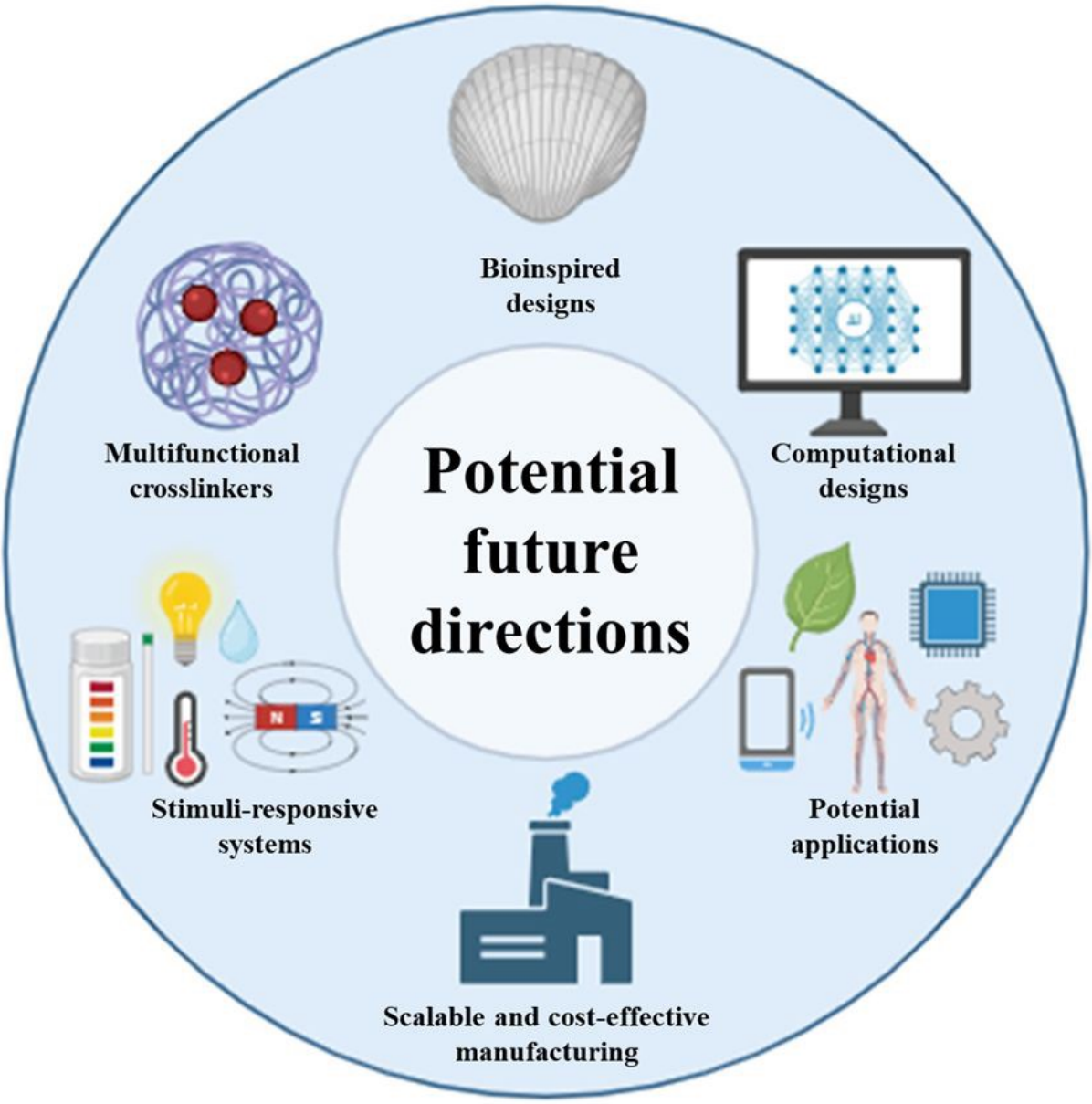

Figure 13. Schematic illustration of potential future research directions for multiple hydrogen-bonded polymeric networks.

View Article Online
DOI: 10.1039/D5LP00189G

CRediT authorship contribution statement

Pouya Rajaee: Writing – review & editing, Writing – original draft, Visualization, Methodology, Formal analysis, Data curation, Conceptualization.

Ishara Wijesinghe: Writing – review & editing.

Zhiyong Li: Writing – review & editing.

Cheng Yan: Writing – review & editing, Validation, Supervision, Formal analysis.

Declaration of competing interest

The authors declare that they have no known competing financial interests or personal relationships that could have appeared to influence the work reported in this paper.

Data availability

No primary research results, software or code have been included and no new data were generated or analysed as part of this review.

Acknowledgments

Pouya Rajaee appreciates the QUT Postgraduate Research Award (QUTPRA), PhD scholarship from Queensland University of Technology, Brisbane, Australia.

References

[1] V.R. Feig, H. Tran, Z. Bao, Biodegradable Polymeric Materials in Degradable Electronic Devices, ACS Cent. Sci., 2018, 4, 337–348.
[2] L. Mandal, B. Verma, P.K. Patel, others, Review on polymer nanocomposite for ballistic & aerospace applications, Mater. Today Proc., 2020.
[3] J.M. Chalovich, E. Eisenberg, Synthetic biodegradable functional polymers for tissue engineering: a brief review, Sci. China Chem., 2014, 57, 490–500.
[4] A. Kl, J. Lei, Bio-inspired design of multiscale structures for function integration, Nano Today, 2011, 6, 155–175.
[5] G. Zhou, L. Li, D.W. Wang, X.Y. Shan, S. Pei, F. Li, H.M. Cheng, A flexible sulfur-graphene-polypropylene separator integrated electrode for advanced Li-S batteries, Adv. Mater., 2015, 27, 641–647.
[6] S. Wan, J. Peng, L. Jiang, Q. Cheng, Bioinspired Graphene-Based Nanocomposites and Their Application in Flexible Energy Devices, Adv. Mater., 2016, 28, 7862–7898.
[7] J. Ge, L. Sun, F.R. Zhang, Y. Zhang, L.A. Shi, H.Y. Zhao, H.W. Zhu, H.L. Jiang, S.H. Yu, A Stretchable Electronic Fabric Artificial Skin with Pressure-, Lateral Strain-, and Flexion-Sensitive Properties, Adv. Mater., 2016, 28, 722–728.
[8] H. Bin Yao, J. Ge, C.F. Wang, X. Wang, W. Hu, Z.J. Zheng, Y. Ni, S.H. Yu, A flexible and highly pressure-sensitive graphene-polyurethane sponge based on fractured microstructure design, Adv. Mater., 2013, 25, 6692–6698.
[9] L.L. Li, G. Bin Qi, F. Yu, S.J. Liu, H. Wang, An adaptive biointerface from self-assembled functional peptides for tissue engineering, Adv. Mater., 2015, 27, 3181–3188.

[10] R.O. Ritchie, The conflicts between strength and toughness, Nat. Mater., 2011, 10, 817–822.
[11] H. Wan, B. Wu, L. Hou, P. Wu, Amphibious Polymer Materials with High Strength and Superb Toughness in Various Aquatic and Atmospheric Environments, Adv. Mater., 2024, 36.
[12] M. Irigoyen, A. Fernandez, A. Ruiz, F. Ruiperez, J.M. Matxain, Diselenide bonds as an alternative to outperform the efficiency of disulfides in self-healing materials, J. Org. Chem., 2019, 84, 4200–4210.
[13] S. Cho, S.Y. Hwang, D.X. Oh, J. Park, Recent progress in self-healing polymers and hydrogels based on reversible dynamic B–O bonds: boronic/boronate esters, borax, and benzoxaborole, J. Mater. Chem. A, 2021, 9, 14630–14655.
[14] G.P. Carden, M.L. Martins, G. Toleutay, S. Ge, B. Li, S. Zhao, A.P. Sokolov, Critical role of free amine groups in the imine bonds exchange in dynamic covalent networks, Macromolecules, 2024, 57, 8621–8631.
[15] J. Canadell, H. Goossens, B. Klumperman, Self-healing materials based on disulfide links, Macromolecules, 2011, 44, 2536–2541.
[16] Y. V. Pereverzev, O. V. Prezhdo, L.R. Dalton, Structural origin of the enhanced electro-optic response of dendrimeric systems, Chem. Phys. Lett., 2003, 373, 207–212.
[17] D. Mozhdehi, S. Ayala, O.R. Cromwell, Z. Guan, Self-healing multiphase polymers via dynamic metal-ligand interactions, J. Am. Chem. Soc., 2014, 136, 16128–16131.
[18] Q. Zhang, S. Niu, L. Wang, J. Lopez, S. Chen, Y. Cai, R. Du, Y. Liu, J.C. Lai, L. Liu, C.H. Li, X. Yan, C. Liu, J.B.H. Tok, X. Jia, Z. Bao, An Elastic Autonomous Self-Healing Capacitive Sensor Based on a Dynamic Dual Crosslinked Chemical System, Adv. Mater., 2018, 30.
[19] A. Sanchez-Sanchez, A. Arbe, J. Colmenero, J.A. Pomposo, Metallo-folded single-chain nanoparticles with catalytic selectivity, ACS Macro Lett., 2014, 3, 439–443.
[20] Z. Li, Y. Shan, X. Wang, H. Li, K. Yang, Y. Cui, Self-healing flexible sensor based on metal-ligand coordination, Chem. Eng. J., 2020, 394.
[21] H. Xie, X. Liu, D. Sheng, H. Wu, Y. Zhou, X. Tian, Y. Sun, B. Shi, Y. Yang, Novel titin-inspired high-performance polyurethanes with self-healing and recyclable capacities based on dual dynamic network, Polymer (Guildf). 2021, 230.
[22] Y. Yao, B. Liu, Z. Xu, J. Yang, W. Liu, An unparalleled H-bonding and ion-bonding crosslinked waterborne polyurethane with super toughness and unprecedented fracture energy, Mater. Horizons, 2021, 8, 2742–2749.
[23] J. Yan, M. Li, Z. Wang, C. Chen, C. Ma, G. Yang, Highly tough, multi-stimuli-responsive, and fast self-healing supramolecular networks toward strain sensor application, Chem. Eng. J., 2020, 389.
[24] B. Liu, Z. Tang, Z. Wang, L. Zhang, B. Guo, Integrating transient and sacrificial bonds into biobased elastomers toward mechanical property enhancement and macroscopically responsive property, Polymer (Guildf). 2019, 184.
[25] M. Ahmadi, S. Seiffert, Coordination Geometry Preference Regulates the Structure and Dynamics of Metallo-Supramolecular Polymer Networks, Macromolecules, 2021, 54, 1388–1400.
[26] C.H. Li, C. Wang, C. Keplinger, J.L. Zuo, L. Jin, Y. Sun, P. Zheng, Y. Cao, F. Lissel, C. Linder, X.Z. You, Z. Bao, A highly stretchable autonomous self-healing elastomer, Nat. Chem., 2016, 8, 618–624.
[27] J.C. Lai, X.Y. Jia, D.P. Wang, Y.B. Deng, P. Zheng, C.H. Li, J.L. Zuo, Z. Bao, Thermodynamically stable whilst kinetically labile coordination bonds lead to strong and tough self-healing polymers, Nat. Commun., 2019, 10.
[28] Y. Sheng, M. Wang, K. Zhang, Z. Wu, Y. Chen, X. Lu, An “inner soft external hard”,

scratch-resistant, self-healing waterborne poly(urethane-urea) coating based on gradient metal coordination structure, Chem. Eng. J., 2021, 426.

[29] Y. Song, Y. Liu, T. Qi, G.L. Li, Towards Dynamic but Supertough Healable Polymers through Biomimetic Hierarchical Hydrogen-Bonding Interactions, Angew. Chemie - Int. Ed., 2018, 57, 13838–13842.

[30] J.-M. Lehn, Supramolecular Chemistry-Scope and Perspectives Molecules, Supermolecules, and Molecular Devices (Nobel Lecture), Angew. Chemie Int. Ed. English, 1988, 27, 89–112.

[31] P. Song, J. Dai, G. Chen, Y. Yu, Z. Fang, W. Lei, S. Fu, H. Wang, Z.G. Chen, Bioinspired Design of Strong, Tough, and Thermally Stable Polymeric Materials via Nanoconfinement, ACS nano, 2018, 12, 9266–9278.

[32] J. Cao, Z. Zhou, Q. Song, K. Chen, G. Su, T. Zhou, Z. Zheng, C. Lu, X. Zhang, Ultrarobust Ti3C2TxMXene-Based Soft Actuators via Bamboo-Inspired Mesoscale Assembly of Hybrid Nanostructures, ACS nano, 2020, 14, 7055–7065.

[33] S. Sun, Y. Xue, X. Xu, L. Ding, Z. Jiang, L. Meng, P. Song, Y. Bai, Highly Stretchable, Ultratough, and Strong Polyesters with Improved Postcrystallization Optical Property Enabled by Dynamic Multiple Hydrogen Bonds, Macromolecules, 2021, 54, 1254–1266.

[34] J.A. Fernández, Exploring hydrogen bond in biological molecules, J. Indian Inst. Sci., 2020, 100, 135–154.

[35] R.E. Hubbard, M.K. Haider, Hydrogen bonds in proteins: role and strength, Encycl. Life Sci. 2010.

[36] P. Kolandaivel, V. Nirmala, Study of proper and improper hydrogen bonding using Bader's atoms in molecules (AIM) theory and NBO analysis, J. Mol. Struct., 2004, 694, 33–38.

[37] X. Zhao, X.Z. Wang, X.K. Jiang, Y.Q. Chen, Z.T. Li, G.J. Chen, Hydrazide-Based Quadruply Hydrogen-Bonded Heterodimers. Structure, Assembling Selectivity, and Supramolecular Substitution, J. Am. Chem. Soc., 2003, 125, 15128–15139.

[38] S.C.C. Van Der Lubbe, F. Zaccaria, X. Sun, C.F. Guerra, Secondary Electrostatic Interaction Model Revised: Prediction Comes Mainly from Measuring Charge Accumulation in Hydrogen-Bonded Monomers, J. Am. Chem. Soc., 2019, 141, 4878–4885.

[39] F.H. Beijer, R.P. Sijbesma, H. Kooijman, A.L. Spek, E.W. Meijer, Strong dimerization of ureidopyrimidones via quadruple hydrogen bonding, J. Am. Chem. Soc., 1998, 120, 6761–6769.

[40] F.H. Beijer, H. Kooijman, A.L. Spek, R.P. Sijbesma, E.W. Meijer, Self-complementarity achieved through quadruple hydrogen bonding, Angew. Chem. Int. Ed., 1998, 37, 75–78.

[41] A.T. Ten Cate, H. Kooijman, A.L. Spek, R.P. Sijbesma, E.W. Meijer, Conformational Control in the Cyclization of Hydrogen-Bonded Supramolecular Polymers, 2004, 126, 3801–3808.

[42] G.B.W.L. Ligthart, H. Ohkawa, R.P. Sijbesma, E.W. Meijer, Complementary quadruple hydrogen bonding in supramolecular copolymers, J. Am. Chem. Soc., 2005, 127, 810–811.

[43] B.J.B. Folmer, R.P. Sijbesma, H. Kooijman, A.L. Spek, E.W. Meijer, Cooperative dynamics in duplexes of stacked hydrogen-bonded moieties, J. Am. Chem. Soc., 1999, 121, 9001–9007.

[44] P.S. Corbin, S.C. Zimmerman, P.A. Thiessen, N.A. Hawryluk, T.J. Murray, Complexation-induced unfolding of heterocyclic ureas. Simple foldamers equilibrate with multiply hydrogen-bonded sheetlike structures, J. Am. Chem. Soc., 2001, 123,

View Article Online
DOI: 10.1039/D5LP00189G

10475–10488.
[45] E.S. Brielle, I.T. Arkin, Quantitative Analysis of Multiplex H-Bonds, J. Am. Chem. Soc., 2020, 142, 14150–14157.
[46] Y. Yang, X. Ding, M.W. Urban, Chemical and physical aspects of self-healing materials, Prog. Polym. Sci. 2015, 34–59.
[47] N. Roy, B. Bruchmann, J.M. Lehn, DYNAMERS: Dynamic polymers as self-healing materials, Chem. Soc. Rev., 2015, 44, 3786–3807.
[48] R. Hou, G. Li, Y. Zhang, M. Li, G. Zhou, X. Chai, Self-Healing Polymers Materials Based on Dynamic Supramolecular Motifs, Prog. Chem., 2019, 31, 690–698.
[49] T. Kawakami, T. Kato, Use of intermolecular hydrogen bonding between imidazolyl moieties and carboxylic acids for the supramolecular self-association of liquid-crystalline side-chain polymers and networks, Macromolecules, 1998, 31, 4475–4479.
[50] L. Liu, M. Zhu, Z. Ma, X. Xu, J. Dai, Y. Yu, S. Mohsen Seraji, H. Wang, P. Song, Small multiamine molecule enabled fire-retardant polymeric materials with enhanced strength, toughness, and self-healing properties, Chem. Eng. J., 2022, 440.
[51] X. Zhang, W. Liu, D. Yang, X. Qiu, Biomimetic Supertough and Strong Biodegradable Polymeric Materials with Improved Thermal Properties and Excellent UV-Blocking Performance, Adv. Funct. Mater., 2019, 29.
[52] D.K. Buslov, N.I. Sushko, O.N. Tretinnikov, IR investigation of hydrogen bonds in weakly hydrated films of poly(vinyl alcohol), Polym. Sci. Ser. A, 2011, 53, 1121–1127.
[53] D.S. Bag, S. Tiwari, K.M. Meenu, Chiral copolymers of (R)-N-(1-phenyl-ethyl) methacrylamide (R-NPEMAM) and 2-hydroxy ethyl methacrylate (HEMA): investigation of physico-chemical behavior, thermal properties and degradation kinetics, J. Polym. Mater., 2023, 40, 105–123.
[54] T. Zhou, F. Chen, C. Tang, H. Bai, Q. Zhang, H. Deng, Q. Fu, The preparation of high performance and conductive poly (vinyl alcohol)/graphene nanocomposite via reducing graphite oxide with sodium hydrosulfite, Compos. Sci. Technol., 2011, 71, 1266–1270.
[55] C.J. Seliskar, R.E. Hoffmann, On the infrared spectrum of malonaldehyde, a tunneling hydrogen-bonded molecule, J. Mol. Spectrosc., 1982, 96, 146–155.
[56] P. Song, Z. Xu, Y. Lu, Q. Guo, Bio-Inspired Hydrogen-Bond Cross-Link Strategy toward Strong and Tough Polymeric Materials, Macromolecules, 2015, 48, 3957–3964.
[57] M. Qian, Y. Sun, X. Xu, L. Liu, P. Song, Y. Yu, H. Wang, J. Qian, 2D-alumina platelets enhance mechanical and abrasion properties of PA612 via interfacial hydrogen-bond interactions, Chem. Eng. J., 2017, 308, 760–771.
[58] S.H. Hwang, D. Kang, R.S. Ruoff, H.S. Shin, Y. Bin Park, Poly(vinyl alcohol) reinforced and toughened with poly(dopamine)-treated graphene oxide, and its use for humidity sensing, ACS nano, 2014, 8, 6739–6747.
[59] Q. Wu, Y. Shangguan, M. Du, J. Zhou, Y. Song, Q. Zheng, Steady and dynamic rheological behaviors of sodium carboxymethyl cellulose entangled semi-dilute solution with opposite charged surfactant dodecyl-trimethylammonium bromide, J. Colloid Interface Sci., 2009, 339, 236–242.
[60] D. Zhao, Z. Zhang, J. Zhao, K. Liu, Y. Liu, G. Li, X. Zhang, R. Bai, X. Yang, X. Yan, A Mortise-and-Tenon Joint Inspired Mechanically Interlocked Network, Angew. Chem. Int. Ed., 2021, 133, 16360–16365.
[61] G.M. Scheutz, J.J. Lessard, M.B. Sims, B.S. Sumerlin, Adaptable Crosslinks in Polymeric Materials: Resolving the Intersection of Thermoplastics and Thermosets, J. Am. Chem. Soc., 2019, 141, 16181–16196.
[62] K. Yu, M. Wang, J. Wu, K. Qian, J. Sun, X. Lu, Modification of the interfacial interaction between carbon fiber and epoxy with carbon hybrid materials, Nanomaterials, 2016, *6*(5), 89.

[63] E.H. Qua, P.R. Hornsby, H.S.S. Sharma, G. Lyons, R.D. Mccall, Preparation and characterization of Poly(vinyl alcohol) nanocomposites made from cellulose nanofibers, J. Appl. Polym. Sci., 2009, 113, 2238–2247.

[64] L. Liu, X. Xu, M. Zhu, X. Cui, J. Feng, Z.F. Rad, H. Wang, P. Song, Bioinspired Strong, Tough, and Biodegradable Poly(Vinyl Alcohol) and its Applications as Substrates for Humidity Sensors, Adv. Mater. Technol., 2023, 8.

[65] P. Song, Z. Xu, Q. Guo, Bioinspired strategy to reinforce PVA with improved toughness and thermal properties via hydrogen-bond self-assembly, ACS Macro Lett., 2013, 2, 1100–1104.

[66] L. Li, X. Xu, L. Liu, P. Song, Q. Cao, Z. Xu, Z. Fang, H. Wang, Water governs the mechanical properties of poly(vinyl alcohol), Polymer (Guildf)., 2021, 213.

[67] L. Liu, M. Zhu, X. Xu, X. Li, Z. Ma, Z. Jiang, A. Pich, H. Wang, P. Song, Dynamic Nanoconfinement Enabled Highly Stretchable and Supratough Polymeric Materials with Desirable Healability and Biocompatibility, Adv. Mater., 2021, 33.

[68] R. Panigrahi, S. Chakraborty, J. Ye, G.S. Lim, F.C.H. Lim, J.K.H. Yam, L.Y. Wu, S. Chng, M. Prawirasatya, A.M. van Herk, P. Thoniyot, Elucidating the Role of Interfacial Hydrogen Bonds on Glass Transition Temperature Change in a Poly(Vinyl Alcohol)/SiO2 Polymer-Nanocomposite by Noncovalent Interaction Characterization and Atomistic Molecular Dynamics Simulations, Macromol. Rapid Commun., 2020, 41.

[69] W. Xie, Q. Bao, Y. Liu, H. Wen, Q. Wang, Hydrogen Bond Association to Prepare Flame Retardant Polyvinyl Alcohol Film with High Performance, ACS Appl. Mater. Interfaces, 2021, 13, 5508–5517.

[70] X. Xu, L. Li, S.M. Seraji, L. Liu, Z. Jiang, Z. Xu, X. Li, S. Zhao, H. Wang, P. Song, Bioinspired, Strong, and Tough Nanostructured Poly(vinyl alcohol)/Inositol Composites: How Hydrogen-Bond Cross-Linking Works?, Macromolecules, 2021, 54, 9510–9521.

[71] P.J. Taenzler, K. Sadeghian, C. Ochsenfeld, Theoretical investigations of the hydrogen bond in a tetraamido/diamino quaternized macrocycle, Mol. Phys. 117 , 2019, 1276–1286.

[72] G. Gunnarsson, H. Wennerström, W. Egan, S. Forsén, Proton and deuterium NMR of hydrogen bonds: Relationship between isotope effects and the hydrogen bond potential, Chem. Phys. Lett. 38 , 1976, 96–99.

[73] R. Konrat, M. Tollinger, G. Kontaxis, B. Kräutler, NMR Techniques to Study Hydrogen Bonding in Aqueous Solution, Hydrog. Bond Res. , 1999, 17–38.

[74] M.M. Coleman, J.F. Graf, P.C. Painter, Specific interactions and the miscibility of polymer blends, Specif. Interact. Miscibility Polym. Blends , 2017, 1–516.

[75] Z. Guo, Y. Qu, C. Tian, M. Su, H.M. Yin, Constructing stretchable, tough, and stiff fluoroelastomer via tannic acid self-assembly, Colloids Surfaces A Physicochem. Eng. Asp., 2023, 666.

[76] J. Chen, J. Jing, C. Wang, T. Chen, J. Xu, B. Yao, J. Fu, Ultra-strong, ultra-tough, and transparent polymer composite with excellent dynamic and biodegradable properties enabled by bicontinuous structure, Polymer (Guildf)., 2023, 283.

[77] T. Kashiwagi, F. Du, J.F. Douglas, K.I. Winey, R.H. Harris, J.R. Shields, Nanoparticle networks reduce the flammability of polymer nanocomposites., Nat. Mater. 4 , 2005, 928–933.

[78] P. Song, L. Xu, Z. Guo, Y. Zhang, Z. Fang, Flame-retardant-wrapped carbon nanotubes for simultaneously improving the flame retardancy and mechanical properties of polypropylene, J. Mater. Chem. 18 , 2008, 5083–5091.

[79] Y. Hu, C.L. Bao, Y.Q. Guo, L. Song, Poly(vinyl alcohol) nanocomposites based on graphene and graphite oxide: a comparative investigation of property and mechanism,

View Article Online
DOI: 10.1039/D5LP00189G

J. Mater. Chem. 21 , 2011, 13942–13950.
[80] P. Rittigstein, R.D. Priestley, L.J. Broadbelt, J.M. Torkelson, Model polymer nanocomposites provide an understanding of confinement effects in real nanocomposites, Nat. Mater. 6 , 2007, 278–282.
[81] X. Qin, W. Xia, R. Sinko, S. Keten, Tuning Glass Transition in Polymer Nanocomposites with Functionalized Cellulose Nanocrystals through Nanoconfinement, Nano Lett. 15 , 2015, 6738–6744.
[82] Y. Guan, W. Li, Y. Zhang, Z. Shi, J. Tan, F. Wang, Y. Wang, Aramid nanofibers and poly (vinyl alcohol) nanocomposites for ideal combination of strength and toughness via hydrogen bonding interactions, Compos. Sci. Technol. 144 , 2017, 193–201.
[83] Y. Shi, C. Liu, L. Liu, L. Fu, B. Yu, Y. Lv, F. Yang, P. Song, Strengthening, toughing and thermally stable ultra-thin MXene nanosheets/polypropylene nanocomposites via nanoconfinement, Chem. Eng. J., 2019, 378.
[84] L. Liu, M. Zhu, Y. Shi, X. Xu, Z. Ma, B. Yu, S. Fu, G. Huang, H. Wang, P. Song, Functionalizing MXene towards highly stretchable, ultratough, fatigue- and fire-resistant polymer nanocomposites, Chem. Eng. J., 2021, 424.
[85] C. Liu, K. Xu, Y. Shi, J. Wang, S. Ma, Y. Feng, Y. Lv, F. Yang, M. Liu, P. Song, Fire-safe, mechanically strong and tough thermoplastic Polyurethane/MXene nanocomposites with exceptional smoke suppression, Mater. Today Phys., 2022, 22.
[86] J. Li, P. Zhang, L. Chen, G. Li, H. Chen, C. Jia, Y. Wu, M. Chen, X. Zhao, P. Song, Strong, tough and healable elastomer nanocomposites enabled by a hydrogen-bonded supramolecular network, Compos. Commun., 2020, 22.
[87] T. Zhang, Q. Yu, L. Fang, J. Wang, T. Wu, P. Song, All-Organic Multilayer Coatings for Advanced Poly(lactic acid) Films with High Oxygen Barrier and Excellent Antifogging Properties, ACS Appl. Polym. Mater. 1 , 2019, 3470–3476.
[88] Y. Fang, J. Tong, S. Qiu, Bioinspired Strong and Tough Poly(ϵ-caprolactone)/Graphene Nanodot Composite Films via Weak Hydrogen Bonds: Implications for Thermal-Mechanical Properties, ACS Appl. Nano Mater. 6 , 2023, 19088–19097.
[89] J. Ding, H. Zhao, S. Shi, J. Su, Q. Chu, H. Wang, B. Fang, M.R. Miah, J. Wang, J. Zhu, High-Strength, High-Barrier Bio-Based Polyester Nanocomposite Films by Binary Multiscale Boron Nitride Nanosheets, Adv. Funct. Mater., 2024, 34.
[90] P. Song, Z. Xu, M.S. Dargusch, Z.G. Chen, H. Wang, Q. Guo, Granular Nanostructure: A Facile Biomimetic Strategy for the Design of Supertough Polymeric Materials with High Ductility and Strength, Adv. Mater., 2017, 29.
[91] S. Xiong, C. Zhang, R. Huang, K. Luo, X. Zhu, G. Tong, Strong yet tough, excellent thermal resistant and UV-Protective Polydopamine/Poly(vinyl alcohol) composites via hydrogen-bonding interaction, Polymer (Guildf)., 2021, 221.
[92] Y. Fang, S. Xiong, H. Huang, J. Zhu, J. Yu, Y. Wang, Z. Hu, Polydopamine nanotube for dual bio-inspired strong, tough, and flame retarding composites, Compos. Part B Eng., 2020, 197.
[93] S. Xie, S. Dai, Visualizing small molecules via transmission electron microscopy, Microstructures, 2025, 5, N-A.
[94] R. Chitas, D.R. Fonseca, P. Parreira, M.C.L. Martins, Targeted nanotherapeutics for the treatment of Helicobacter pylori infection, J. Biomed. Sci., 2024, 31, 78.
[95] F. Cerrón-Mercado, B.K. Salva-Ruíz, D. Nolazco-Cama, C. Espinoza-Silva, J. Fernández-López, J.A. Pérez-Alvarez, M. Viuda-Martos, Development of chincho (Tagetes elliptica Sm.) essential oil organogel nanoparticles through ionic gelation and process optimization with Box–Behnken design, Gels, 2022, 8, 815.
[96] B.R. Maciel, K. Wang, M. Müller, C. Oelschlaeger, N. Willenbacher, Targeted micro-phase separation–a generic design concept to control the elasticity of extrudable

View Article Online
DOI: 10.1039/D5LP00189G

hydrogels, Mater. Des., 2023, 227, 111803.
[97] T. Zhao, J. Wang, Y. Liu, X. Li, Y. Bai, B. Luo, S. Nie, Self-healing and toughness triboelectric materials enabled by dynamic nanoconfinement quenching, Adv. Funct. Mater., 2024, 34, 2410096.
[98] Z. Xie, B.L. Hu, R.W. Li, Q. Zhang, Hydrogen bonding in self-healing elastomers, ACS Omega, 2021, 6, 9319–9333.
[99] O. Lebel, T. Maris, M.È. Perron, E. Demers, J.D. Wuest, The dark side of crystal engineering: creating glasses from small symmetric molecules that form multiple hydrogen bonds, J. Am. Chem. Soc., 2006, 128, 10372–10373.
[100] C.B. St. Pourcain, A.C. Griffin, Thermoreversible supramolecular networks with polymeric properties, Macromolecules, 1995, 28, 4116–4121.
[101] Z. Zhang, J. Luo, S. Zhao, S. Ge, J.M. Carrillo, J.K. Keum, C. Do, S. Cheng, Y. Wang, A.P. Sokolov, P.F. Cao, Surpassing the stiffness-extensibility trade-off of elastomers via mastering the hydrogen-bonding clusters, Matter, 2022, 5, 237–252.
[102] S.V. Wanasinghe, O.J. Dodo, D. Konkolewicz, Dynamic bonds: adaptable timescales for responsive materials, Angew. Chem., 2022, 134, e202206938.
[103] M.L. Martins, X. Zhao, Z. Demchuk, J. Luo, G.P. Carden, G. Toleutay, A.P. Sokolov, Viscoelasticity of polymers with dynamic covalent bonds: concepts and misconceptions, Macromolecules, 2023, 56, 8688–8696.
[104] X. Hu, M. Vatankhah-Varnoosfaderani, J. Zhou, Q. Li, S.S. Sheiko, Weak hydrogen bonding enables hard, strong, tough, and elastic hydrogels, Adv. Mater., 2015, 27, 6899–6905.
[105] S. Thiele, C.J. Plummer, L. Piveteau, H. Frauenrath, Dynamics of hydrogen-bonded end groups in bulk polymers revealed by solid-state NMR spectroscopy relaxation dispersion experiments, Commun. Chem., 2025, 8, 217.
[106] Y.W. Ge, J.W. Lu, Z.Y. Sun, Z.Q. Liu, J. Zhou, Q.F. Ke, Y.Q. Mao, Y.P. Guo, Z.A. Zhu, Ursolic acid loaded-mesoporous bioglass/chitosan porous scaffolds as drug delivery system for bone regeneration, Nanomedicine Nanotechnology, Biol. Med., 2019, 18, 336–346.
[107] X. Yu, Y. Wang, X. Liu, Y. Ge, S. Zhang, Ursolic acid loaded-mesoporous hydroxylapatite/ chitosan therapeutic scaffolds regulate bone regeneration ability by promoting the m2-type polarization of macrophages, Int. J. Nanomedicine, 2021, 16, 5301–5315.
[108] J. Cao, C. Lu, J. Zhuang, M. Liu, X. Zhang, Y. Yu, Q. Tao, Multiple Hydrogen Bonding Enables the Self-Healing of Sensors for Human–Machine Interactions, Angew. Chemie - Int. Ed., 2017, 56, 8795–8800.
[109] T. Munaoka, X. Yan, J. Lopez, J.W.F. To, J. Park, J.B.H. Tok, Y. Cui, Z. Bao, Ionically Conductive Self-Healing Binder for Low Cost Si Microparticles Anodes in Li-Ion Batteries, Adv. Energy Mater. 2018, 8.
[110] J.F. Baumhauer, D. Singh, M. Glazebrook, C. Blundell, G. De Vries, I.L. Le, on behalf of the CARTIVA Motion Study Group, Prospective, randomized, multi-centered clinical trial assessing safety and efficacy of a synthetic cartilage implant versus first metatarsophalangeal arthrodesis in advanced hallux rigidus, Foot Ankle Int., 2016, 37, 457–469.
[111] D. Murugan, H. Arumugam, S. Arumugam, M. Mani, S. Kannan, Superparamagnetic freeze-thawed PVA hydrogel for applications in tissue engineering, drug delivery and bioimaging, Colloids Surf. A Physicochem. Eng. Asp., 2024, 690, 133790.
[112] G.C. Stevens, Living dielectrics, IEEE Electr. Insul. Mag., 2023, 39, 7–33.
[113] L. Pernigoni, A.M. Grande, Towards safer space suits with self-healing materials, in: 16th Eur. Conf. Spacecr. Struct. Mater. Environ. Test. (ECSSMET 2021), 2021, pp. 1–

View Article Online
DOI: 10.1039/D5LP00189G

7.
[114] Z.C. Jiang, Y.Y. Xiao, Y. Kang, B.J. Li, S. Zhang, Semi-IPNs with moisture-triggered shape memory and self-healing properties, Macromol. Rapid Commun., 2017, 38, 1700149.
[115] M. Liu, P. Liu, G. Lu, Z. Xu, X. Yao, Multiphase-assembly of siloxane oligomers with improved mechanical strength and water-enhanced healing, Angew. Chem., 2018, 130, 11412–11416.
[116] K. Wei, X. Yu, X. Zhang, J. Cao, L. Bai, W. Wang, L. Yang, Self-healing, tough hydrogels with long-lasting moisture and extreme temperature tolerance and application for flexible sensors, Chem. Eng. Sci., 2025, 122312.
[117] M.C. Luo, J. Zeng, X. Fu, G. Huang, J. Wu, Toughening diene elastomers by strong hydrogen bond interactions, Polymer, 2016, 106, 21–28.

View Article Online
DOI: 10.1039/D5LP00189G

Data Availability Statement

No primary research results, software or code have been included and no new data were generated or analysed as part of this review.